



DEPARTMENT OF ECONOMICS
AND BUSINESS ECONOMICS
AARHUS UNIVERSITY



Modelling and Estimating Large Macroeconomic Shocks During the Pandemic

Luisa Corrado, Stefano Grassi and Aldo Paolillo

CREATES Research Paper 2021-08

Modelling and Estimating Large Macroeconomic Shocks During the Pandemic*

Luisa Corrado[†] Stefano Grassi[‡] Aldo Paolillo[§]

June 11, 2021

Abstract

This paper proposes and estimates a new Two-Sector One-Agent model that features large shocks. The resulting medium-scale New Keynesian model includes the standard real and nominal frictions used in the empirical literature and allows for heterogeneous COVID-19 pandemic exposure across sectors. We solve the model nonlinearly and we propose a new nonlinear, non-Gaussian filter designed to handle large pandemic shocks to make inference feasible. Monte Carlo experiments show that it correctly identifies the source and time location of shocks with a massively reduced running time, making the estimation of macro-models with disaster shocks feasible. The estimation is carried out using the Sequential Monte Carlo sampler recently proposed by [Herbst and Schorfheide \(2014\)](#).

Our empirical results show that the pandemic-induced economic downturn can be reconciled with a combination of large demand and supply shocks. More precisely, starting from the second quarter of 2020, the model detects the occurrence of a large negative demand shock in consuming all kinds of goods, together with a large negative demand shock in consuming contact-intensive products. On the supply side, our proposed method detects a large labor supply shock to the general sector and a large labor productivity shock in the pandemic-sensitive sector.

JEL codes: C11, C51, E30.

Keywords: COVID-19, Nonlinear, Non-Gaussian, Large shocks, DSGE.

*Stefano Grassi gratefully acknowledges financial support from the University of Rome ‘Tor Vergata’ under Grant “Beyond Borders” (CUP: E84I20000900005).

[†]University of Rome ‘Tor Vergata’ - Department of Economics and Finance. Email: luisa.corrado@uniroma2.it

[‡]University of Rome ‘Tor Vergata’ - Department of Economics and Finance and CREATES - Aarhus University. Email: stefano.grassi@uniroma2.it

[§]University of Rome ‘Tor Vergata’ - Department of Economics and Finance. Email: aldo.paolillo@uniroma2.it

1 Introduction

The COVID-19 pandemic outbreak that occurred in 2020 is prompting new and unexpected research challenges. The drastic containment policies and the social responses to the pandemic have resulted in a sudden worldwide economic disruption, consisting in one of the most severe global recessions since the Great Depression. The macroeconomic effects are unprecedented both in nature and in magnitude and require the development of new economic models and methods or the adaptation of existing methods, see [Lenza and Primiceri \(2020\)](#).

From a macroeconomic standpoint, the COVID-19 pandemic raises questions about its possible classification into a supply or a demand shock, because both production and consumption possibilities are impaired. Indeed, health concerns in contact-intensive economic activities hinder the scope for either producing and consuming goods and services safely. In addition to the first-order effects, stemming from the inability to supply or consume products safely, cascading effects can also emerge. Among others, income and substitution effects resulting from foregone consumption of pandemic-sensitive goods can exacerbate economic losses, for reasons above and beyond the ones related to public health.

This paper contributes to the emerging literature on the economic effects of the pandemic by bridging a structural macroeconomic model with the data. In this respect one key contribution of this paper is to build and estimate a new medium-scale New Keynesian dynamic stochastic general equilibrium (NK-DSGE) that features disaster shocks. Our model also includes the usual features of a DSGE model to be suited for an empirical purpose: nominal frictions in prices and wages, real frictions on investment, variable capital utilization, habits in consumption and a zero-lower bound (ZLB) on the nominal interest rate.

The model is estimated using U.S. time series, which include the COVID-19 periods and allow us to identify the economic nature of the pandemic shocks. As the economic impact of social distancing and containment policies has shown to be largely asymmetric across industries, the model includes two sectors that have different degrees of exposure to the pandemic. In the data, we identify the most affected sector as the *U.S. Leisure and Hospitality* sector according to the BEA/BLS industry classification and the (relatively) less

affected sector as the *rest of the economy*.^{*} To capture the salient feature of pandemic shocks, our model considers large shocks both in demand for pandemic-sensitive products and in demand from the unaffected sector. Moreover, we study big shocks in labor supply and productivity in both sectors and how they jointly affect the macro-economy. To accommodate the large movements in the time series during the COVID-19 outbreak, we allow demand and supply shocks to be occasionally drawn from various large shock components, accommodating an inflated variability for some of them. It is important to emphasize that shocks can feedback on each other. As wages for work decline, there will be potentially larger second-order negative effects on demand and the possibility of a self-reinforcing downward spiral in production, employment, income, and demand. We solve the model nonlinearly and, to make inference, we propose a new nonlinear, non-Gaussian filter designed to handle and identify the large pandemic shocks. The key contribution of our filter is to provide an endogenous estimate of both the ex-ante probability of a large shock together with the DSGE parameters. Moreover, our proposed filter is able to distinguish between cases in which the large shock arises either from just one component, some combination of shocks or all of the shocks. Our results show that the economic disruption caused by the pandemic can be explained by a combination of large shocks both on the demand and the supply side. More precisely, starting from the second quarter of 2020, the filter detects the occurrence of a large negative demand shock to the utility of consuming all kinds of goods, together with a large negative demand shock which is specific to the utility of consuming the contact-intensive products. On the supply side, our proposed method can detect a large labor supply shock to the general sector and a large labor productivity shock in the pandemic-sensitive sector.

Our paper relates and contributes to three strands of the literature: the theoretical analysis on the economic effects of the Coronavirus pandemic; the empirical literature that fits time-series models to pandemic related data; and the methodological research on the use of nonlinear, non-Gaussian filter designed to handle rare disaster shocks.

On the theoretical side, the paper is firstly related to the literature on the role of sectoral heterogeneity in the transmission of pandemic-induced shocks. [Guerrieri et al. \(2020\)](#) use

^{*}In a recent contribution [del Rio-Chanona et al. \(2020\)](#) find that these effects vary widely between different industries. While they do not find negative value-added effects for less affected industries such as legal services, power generation, and distribution, or scientific research, the expected loss of value-added reaches up to 80% for leisure and hospitality (accommodation, food services, and independent artists).

a stylized production economy model to assess whether a supply shock (in their case a reduction in labor supply) can trigger demand deficiencies larger than the supply shock itself. In their paper, a key result is that these kinds of shocks, referred to as *Keynesian supply shocks*, can take place in a multisectoral model, but not in a single sector set-up. The rationale is that when one of the two sectors shuts down, a low enough substitutability between the products of the two sectors can decrease the demand for goods in the unaffected sector also. Such a result is facilitated when the credit market is incomplete and when complementarities arise from both technology and preferences. The role of complementarities in production in exacerbating or mitigating the effects of supply and demand shocks is further explored by [Baqae and Farhi \(2021\)](#) in the framework of a rich input-output production network. [Woodford \(2020\)](#) shows that in a multi-sectoral model with incomplete financial markets, the circular flow in the network of payments can be altered as a result of supply disruptions, which are concentrated in some sectors, leading to inefficient demand even without the assumption of complementarities in preferences and technology. Our paper abstracts from complementarities in production and imperfect financial markets but allows us to consider the effects of preferences and rigidities in the transmission of shocks.

This paper is also connected to the literature that deals with the economic effects of the pandemic by using calibrated DSGE models. [Faria-e Castro \(2021\)](#) models the pandemic shock as a negative shock to the utility of services, in the context of a two-sector DSGE with borrowing constraints, to analyze the effectiveness of various fiscal policies. In his calibrated setting, a sequence of utility shocks is fed into the model to mimic the observed series of U.S. unemployment and to build a counterfactual with respect to the realized series of fiscal interventions. On the contrary, [Fornaro and Wolf \(2020a,b\)](#) model the pandemic as a negative shock to total factor productivity, which can generate long-lasting economic losses in the framework of a New Keynesian DSGE with endogenous growth. In the two aforementioned contributions, one kind of pandemic-related shock is allowed one at a time. Differently from their set-up, our model allows the pandemic to result in different types of shocks that hit together the economy and to quantitatively assess the relative importance of them. The skeleton of our model is very similar to that of [Abo-Zaid and Xuguang \(2020\)](#) who build a New Keynesian model with two sectors affected differently

by the epidemic. The shocks associated with the pandemic are the same as ours (except for the fact that on the production side their model does not allow the pandemic to affect labor supply and labor productivity at the same time). In the present paper, the model of [Abo-Zaid and Xuguang \(2020\)](#) is enriched by additional features to fit the data, in the spirit of [Christiano et al. \(2005\)](#) and [Smets and Wouters \(2003\)](#): the presence of capital and related frictions; variable capital utilization; imperfect competition and wage rigidities in labor markets; habits in consumption; a zero-lower bound on the nominal interest rate. Another part of the literature focuses on integrating an epidemiological model with the economic one including, among others, [Eichenbaum et al. \(2020a,b\)](#), [Bodenstein et al. \(2020\)](#) and [Kaplan et al. \(2020\)](#). We consider, instead, the pandemic shocks as exogenous since the optimal trade-off between health and economic activity is outside the focus of the paper.

On the empirical side, the present paper is related to the contributions involved in fitting time series models to pandemic-related data. [Brinca et al. \(2020\)](#) use a Bayesian structural vector autoregression (Bayesian SVAR) to disentangle labor supply and demand shocks across U.S. industries during the first months of 2020. They fit a SVAR model using data on hours worked and real wages up to February 2020 and perform a historical shock decomposition for the following months of 2020, given the estimated parameters. They find that COVID-19 resulted in a combination of either demand and supply shocks and that significant heterogeneity appears in the relative importance of the two shocks across sectors. In contrast, [Lenza and Primiceri \(2020\)](#) show that it is possible to estimate a VAR without discarding the extreme movements of 2020. To do so, as in our paper, they allow for the possibility of large shocks, consisting of a lifted standard deviation of innovations. As will be discussed in Section 3, we differ from [Lenza and Primiceri \(2020\)](#) by exploiting the structural nature of our DSGE model to test for the occurrence of just some combination of large shocks, instead of necessarily all of them together.

From a methodological standpoint, this paper is connected with the filtering and estimation of DSGE models. Among others, [Fernández-Villaverde and Rubio-Ramírez \(2007\)](#), [Fernández-Villaverde et al. \(2011\)](#) and [Flury and Shephard \(2011\)](#) apply the Particle Filter (PF) to DSGE estimation, while deterministic filters such as: Central Difference Kalman Filter (CDKF); Unscented Kalman Filter (UKF); and Quadratic Kalman Filter (QKF)

have been used by [Andreasen \(2012, 2013\)](#), [Ivashchenko \(2014\)](#), [Kollmann \(2015\)](#), [Noh \(2019\)](#) and [Benigno et al. \(2020\)](#).

The possibility of large disaster shocks, which call for considering higher-order and interaction effects between variables, requires a nonlinear solution that brings us to a nonlinear non-Gaussian state-space model. In this case, the standard Kalman Filter (KF) cannot be applied and nonlinear non-Gaussian filter, such as the PFs, are needed to approximate the likelihood and filter out the latent states. Unfortunately, PFs become quickly computationally unfeasible, due to the increasing number of state variables. The presence of large shocks (economics disaster) represents an additional blow to the effectiveness of PFs. Large shocks require an enormous number of particles to describe all the possible outcomes that may occur after a disaster shock, see [Pitt and Shephard \(1999\)](#) and [Amisano and Tristani \(2011\)](#).

To solve this issue in a computationally reasonable amount of time, we propose a new nonlinear, non-Gaussian filter that is based on Mixtures of Mixtures of Cubature Kalman Filter (MM-CKF). The Cubature Kalman Filter (CKF) of [Arasaratnam and Haykin \(2009\)](#), is a nonlinear filter that has been used with great success in engineering application. Although similar to the UKF ([Wan and Van Der Merwe, 2000](#)) it is more stable, accurate and allows for a square-root solution that further improve its stability, see [Arasaratnam and Haykin \(2009\)](#). The MM-CKF proposed in this paper runs banks of CKFs in parallel and tests the location and plausibility of each (possible) combination of large and ordinary (not large) shocks. To avoid an exponential growth of the number of filtering components, a collapsing procedure that keeps just the mixands with the largest weights is proposed. To the best of our knowledge, the closest filter to ours is given in [Binning and Maih \(2015\)](#). They use mixtures of Gaussian filters, including the CKF, in the setting of a regime-switching DSGE model: differently from our paper, they stick to an exercise with calibrated parameters and leave estimation outside.

Extensive Monte Carlo experiments show that the MM-CKF correctly identifies the type and time location of shocks with a massively reduced running time, allowing the estimation of DSGE models, featuring large shocks, in a reasonable amount of time. Inference on model parameters uses the Sequential Monte Carlo (SMC) sampler, proposed by [Creal \(2007\)](#) and [Herbst and Schorfheide \(2014, 2015\)](#). This estimation strategy has big advan-

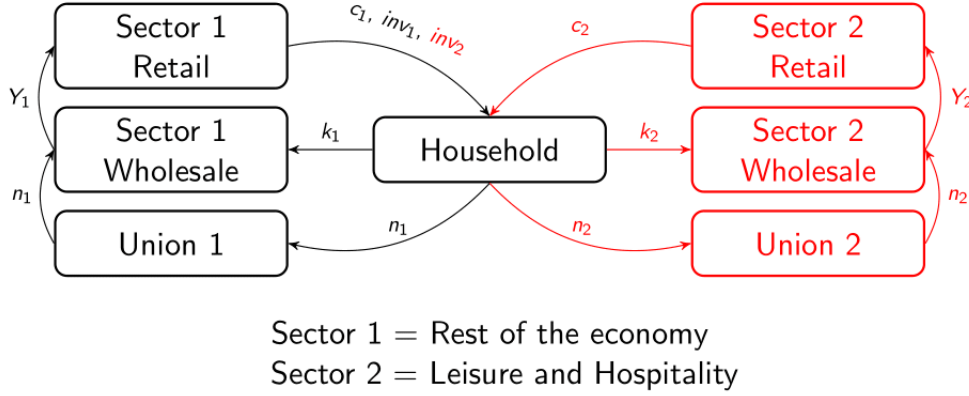


Figure 1: The flow chart of the two-sector one-household model.

tages in terms of parallelization, possible multimodality detection and online estimation updating, as pointed out by [Herbst and Schorfheide \(2014\)](#) and [Cai et al. \(2021\)](#).

The remainder of the paper is organized as follows. Section 2 describes the new Two-Sector One-Agent model that features large shocks. Section 3 discusses the large shocks specification and the model solution. Section 4 discusses filtering problems in the presence of disaster shocks. Section 5 presents the new filtering with Monte Carlo experiments. Section 6 estimates the model on USA data. Finally, Section 7 concludes.

2 Model Description

In the baseline two-sector one-household model, the economy is composed of households, one wholesale and one retail firm in each of the two sectors, unions and the central bank. Figure 1 shows that households consume two final goods from a general sector and a pandemic sensitive sector (Leisure and Hospitality). They also supply labor and rent capital to the wholesale firms in the two sectors. The wholesale firms operate the production technologies and sell the products to the retail firms, which set prices in the monopolistically competitive final goods markets. Unions act as intermediaries between the household and the wholesale firms and introduce contractual wage stickiness in the two sectors. Finally, the central bank is responsible for conducting monetary policy. In the following, the general sector will be denoted as Sector 1 (\mathcal{S}_1), while the Leisure and Hospitality sector will be indicated as Sector 2 (\mathcal{S}_2).

Households

A continuum of measure 1 of households chooses the sequence of consumption for the two goods $c_{1,t}$ and $c_{2,t}$, the sequence of hours to be worked in the two sectors $n_{1,t}$ and $n_{2,t}$, the amount of next period capital in the two sectors $k_{1,t}$ and $k_{2,t}$, and the fractions of capital to be used in production $uk_{1,t}$ and $uk_{2,t}$ so as to maximize lifetime utility:

$$\mathbb{E}_0 \sum_{t=0}^{\infty} \beta^t a_{\zeta,t} \left[\frac{1-h_1}{1-\beta h_1} \log(c_{1,t} - h_1 c_{1,t-1}) + a_{j,t} \frac{1-h_2}{1-\beta h_2} \log(c_{2,t} - h_2 c_{2,t-1}) - \phi_{1,t} \frac{n_{1,t}^{1+\nu_1}}{1+\nu_1} - \phi_{2,t} \frac{n_{2,t}^{1+\nu_2}}{1+\nu_2} \right]. \quad (1)$$

Above, h_1 and h_2 are the external habits parameters, $a_{\zeta,t}$ is the discount factor shock, $a_{j,t}$ is the good 2 preference shock, which affects the relative utility of the two products, and $\phi_{1,t}$ and $\phi_{2,t}$ are the labor supply shocks in the two sectors. The four shocks play a relevant role as exogenous determinants of the pandemic-induced economic losses: large positive shocks to $\phi_{1,t}$ and $\phi_{2,t}$ mirror large rises in labor disutility of working, due to health reasons; a large negative shock to $a_{j,t}$ will drive down the relative utility of consuming goods from the pandemic-affected sector; finally, a large negative shock to $a_{\zeta,t}$ represents a general intertemporal preferences shock that impacts the desire to postpone consumption of both goods. For these reasons, the aforementioned shocks are allowed to be large shocks, see Section 3.

The maximization is conducted subject to the sequence of budget constraints expressed in real terms as:

$$\begin{aligned} c_{1,t} + p_{2,t}c_{2,t} + k_{1,t} + p_{2,t}k_{2,t} + b_t = & \left(\frac{R_{t-1}b_{t-1}}{\pi_{1,t}} \right) + \left(\frac{w_{1,t}n_{1,t}}{X_{w_1,t}} \right) + \left(p_{2,t} \frac{w_{2,t}n_{2,t}}{X_{w_2,t}} \right) \\ & + k_{1,t-1} (1 - \delta_{k_1} + uk_{1,t}r_{k_1,t}) \\ & + p_{2,t}k_{2,t-1} (1 - \delta_{k_2} + uk_{2,t}r_{k_2,t}) - \Psi_{k_1,t} - p_{2,t}\Psi_{k_2,t} \\ & + \Pi_{u_1,t} + p_{2,t}\Pi_{u_2,t} + \Pi_{r_1,t} + p_{2,t}\Pi_{r_2,t} - \Psi_{u_1,t} - p_{2,t}\Psi_{u_2,t}. \end{aligned} \quad (2)$$

In the budget constraint, equation (2), $\Pi_{r_1,t}$, $\Pi_{r_2,t}$, $\Pi_{u_1,t}$ and $\Pi_{u_2,t}$ are, respectively, profits from retailers and profits from unions, which are all taken as a lump sum by the household and are derived in the next subsection from the union optimization problem. The gross inflation rate of the numeraire, $P_{1,t}/P_{1,t-1}$, is denoted by $\pi_{1,t}$, while the relative price of the second final good in terms of the first one, $P_{2,t}/P_{1,t}$, by $p_{2,t}$. The terms $X_{w_1,t}$ and $X_{w_2,t}$ are the wage markups that play the role of a wedge between the wage paid by

the wholesale firms and the wage received by the household, which is collected by labor unions, who are responsible of enforcing monopolistic competition in the labor market. The variables $\Psi_{k_1,t}$, $\Psi_{k_2,t}$, $\Psi_{u_1,t}$ and $\Psi_{u_2,t}$ denote capital adjustment costs and utilization adjustment costs, whose functional expressions are given by:

$$\Psi_{k_1,t} = \frac{\eta_{k_1}}{2} \left(\frac{k_{1,t}}{k_{1,t-1}} - 1 \right)^2 k_{1,t-1}, \quad (3)$$

$$\Psi_{k_2,t} = \frac{\eta_{k_2}}{2} \left(\frac{k_{2,t}}{k_{2,t-1}} - 1 \right)^2 k_{2,t-1}, \quad (4)$$

$$\Psi_{u_1,t} = \left(\frac{1}{\beta} - (1 - \delta_{k_1}) \right) \left[\frac{\left(\frac{\eta_{u_1}}{1 - \eta_{u_1}} \right)}{2} + \frac{\left(\frac{\eta_{u_1}}{1 - \eta_{u_1}} \right)}{2} uk_{1,t}^2 + uk_{1,t} \left(1 - \frac{\eta_{u_1}}{1 - \eta_{u_1}} \right) - 1 \right], \quad (5)$$

$$\Psi_{u_2,t} = \left(\frac{1}{\beta} - (1 - \delta_{k_2}) \right) \left[\frac{\left(\frac{\eta_{u_2}}{1 - \eta_{u_2}} \right)}{2} + \frac{\left(\frac{\eta_{u_2}}{1 - \eta_{u_2}} \right)}{2} uk_{2,t}^2 + \left(1 - \frac{\eta_{u_2}}{1 - \eta_{u_2}} \right) uk_{2,t} - 1 \right]. \quad (6)$$

Optimization leads to the following first order conditions:

- Euler equation:

$$uc_{1,t} = \beta R_t \mathbb{E}_t \left(\frac{uc_{1,t+1}}{\pi_{1,t+1}} \right). \quad (7)$$

- Intratemporal consumption condition:

$$\frac{uc_{2,t}}{p_{2,t}} = uc_{1,t}. \quad (8)$$

- Labor supply to \mathcal{S}_1 :

$$a_{\zeta,t} \phi_{1,t} n_{1,t}^{\nu_1} = \frac{w_{1,t} uc_{1,t}}{X_{w_1,t}}. \quad (9)$$

- Labor supply to \mathcal{S}_2 :

$$a_{\zeta,t} \phi_{2,t} n_{2,t}^{\nu_2} = \frac{w_{2,t} uc_{2,t}}{X_{w_2,t}}. \quad (10)$$

- Capital supply to \mathcal{S}_1 :

$$\begin{aligned} & uc_{1,t} \left[1 + \eta_{k_1} \left(\frac{k_{1,t}}{k_{1,t-1}} - 1 \right) \right] \\ & = \beta \mathbb{E}_t uc_{1,t+1} \left[1 - \delta_{k_1} + r_{k_1,t+1} uk_{1,t+1} + \frac{\eta_{k_1}}{2} \left(\frac{k_{1,t+1}^2}{k_{1,t}^2} - 1 \right) \right]. \end{aligned} \quad (11)$$

- Capital supply to \mathcal{S}_2 :

$$\begin{aligned} p_{2,t}uc_{1,t} & \left[1 + \eta_{k_2} \left(\frac{k_{2,t}}{k_{2,t-1}} - 1 \right) \right] \\ & = \beta \mathbb{E}_t p_{2,t+1} uc_{1,t+1} \left[1 - \delta_{k_2} + r_{k_2,t+1} uk_{2,t+1} + \frac{\eta_{k_2}}{2} \left(\frac{k_{2,t+1}^2}{k_{2,t}^2} - 1 \right) \right]. \end{aligned} \quad (12)$$

- Capital utilization in \mathcal{S}_1 condition:

$$\frac{r_{k_1,t}}{\frac{1}{\beta} - (1 - \delta_{k_1})} = 1 - \frac{\eta_{u,1}}{1 - \eta_{u,1}} + \frac{\eta_{u,1}}{1 - \eta_{u,1}} uk_{1,t}. \quad (13)$$

- Capital utilization in \mathcal{S}_2 condition

$$\frac{r_{k_2,t}}{\frac{1}{\beta} - (1 - \delta_{k_2})} = 1 - \frac{\eta_{u,2}}{1 - \eta_{u,2}} + \left(\frac{\eta_{u,2}}{1 - \eta_{u,2}} \right) uk_{2,t}. \quad (14)$$

where the marginal utilities of consumption are defined by:

$$uc_{1,t} = \frac{1 - h_1}{1 - \beta h_1} \left(\frac{a_{\zeta,t}}{c_{1,t} - h_1 c_{1,t-1}} - \mathbb{E}_t \frac{h_1 \beta a_{\zeta,t+1}}{c_{1,t+1} - h_1 c_{1,t}} \right), \quad (15)$$

$$uc_{2,t} = \frac{1 - h_2}{1 - \beta h_2} \left[\frac{a_{\zeta,t} a_{j,t}}{c_{2,t} - h_2 c_{2,t-1}} - \mathbb{E}_t \left(\frac{h_2 \beta a_{\zeta,t+1} a_{j,t+1}}{c_{2,t+1} - h_2 c_{2,t}} \right) \right]. \quad (16)$$

Equation (7) is the Euler equation with respect to the first good, equation (8) is the intratemporal condition between the two goods, equations (9) and (10) are the labor supply conditions, (11) and (12) pin down capital supply, while (13) and (14) are the capital utilization conditions.

Firms

Similarly to [Bernanke et al. \(1999\)](#), we distinguish between competitive wholesale firms that operate the production technology and charge flexible wholesale prices and retail firms that differentiate the final goods. The wholesale firm rents capital from households and labor from unions, taking the input prices as given in order to maximize:

$$\max P_{1,t}^w Y_{1,t} + P_{2,t}^w Y_{2,t} - \left(\sum_{i=1,2} P_{i,t} w_{i,t} n_{i,t} + \sum_{i=1,2} P_{i,t} r_{k_i,t} uk_{i,t} k_{i,t-1} \right), \quad (17)$$

subject to the production technologies:

$$Y_{1,t} = (a_{z_1,t} n_{1,t})^{1-\alpha_1} (uk_{1,t} k_{1,t-1})^{\alpha_1}, \quad (18)$$

$$Y_{2,t} = (a_{z_2,t} n_{2,t})^{1-\alpha_2} (uk_{2,t} k_{2,t-1})^{\alpha_2}. \quad (19)$$

By dividing Equation (17) by the numeraire $P_{1,t}$, the objective function can be formulated in real terms:

$$\max \frac{Y_{1,t}}{X_{1,t}} + p_{2,t} \frac{Y_{2,t}}{X_{2,t}} - \left[\sum_{i=1,2} \left(\frac{P_{i,t}}{P_{1,t}} \right) w_{i,t} n_{i,t} + \sum_{i=1,2} \left(\frac{P_{i,t}}{P_{1,t}} \right) r_{k_{i,t}} uk_{i,t} k_{i,t-1} \right], \quad (20)$$

Above, $X_{1,t} = \frac{P_{1,t}}{P_{1,t}^w}$ is the markup between the wholesale price $P_{1,t}^w$ and the final goods price $P_{1,t}$ and $X_{2,t} = \frac{P_{2,t}}{P_{2,t}^w}$ is the markup between the wholesale price $P_{2,t}^w$ and $P_{2,t}$. The variables $a_{z_1,t}$ and $a_{z_2,t}$ represent labor productivities in the two sectors. Since a pandemic is likely to hinder the possibility of using labor to produce goods in a safe manner, we allow also labor productivities to be subject to large shocks.

First order conditions lead to the following equations:

- Labor demand by \mathcal{S}_1 :

$$\frac{(1 - \alpha_1) Y_{1,t}}{X_{1,t}} = w_{1,t} n_{1,t}. \quad (21)$$

- Labor demand by \mathcal{S}_2 :

$$\frac{(1 - \alpha_2) Y_{2,t}}{X_{2,t}} = w_{2,t} n_{2,t}. \quad (22)$$

- Capital demand by \mathcal{S}_1 :

$$\frac{\alpha_1 Y_{1,t}}{X_{1,t}} = r_{k_{1,t}} uk_{1,t} k_{1,t-1}. \quad (23)$$

- Capital demand by \mathcal{S}_2 :

$$\frac{\alpha_2 Y_{2,t}}{X_{2,t}} = r_{k_{2,t}} uk_{2,t} k_{2,t-1}. \quad (24)$$

Equations (21) and (22) are the labor demand conditions, while (23) and (24) govern capital demand.

Retailers buy intermediate goods $Y_{1,t}$ and $Y_{2,t}$ at prices $P_{1,t}^w$ and $P_{2,t}^w$ and differentiate them at no cost into a continuum of varieties with constant elasticity of substitution equal to ϵ_{π_1} and ϵ_{π_2} respectively. Households demand each variety j of good $i = 1, 2$ according

to $Y_{i,t}(j) = \left(\frac{P_{i,t}(j)}{P_{i,t}}\right)^{-\epsilon_{\pi_i}} Y_{i,t}^d$ and then reaggregate them in the final consumption and investment goods. Retailers face quadratic adjustment costs à la Rotemberg, so that price stickiness is induced. The adjustment costs are taken with respect to a weighted geometric average of steady-state inflation and last quarter inflation (with relative weights depending on the indexation parameter ι_{π}).

The retail firm problem is therefore to set $P_{i,t}(j)$ so as to maximize:

$$\mathbb{E}_0 \sum_{t=0}^{\infty} \beta^t \left\{ \frac{uc_{1,t}}{uc_{1,0}} \left[\frac{P_{i,t}(j)}{P_{i,t}} Y_{i,t}(j) - \frac{1}{X_{i,t}} Y_{i,t}(j) - \frac{\eta_i}{2} \left(\frac{P_{i,t}(j)}{P_{i,t-1}(j)} - \pi_{i,t-1}^{\iota_{\pi}} \right)^2 Y_{i,t} \right] \right\}, \quad (25)$$

subject to:

$$Y_{i,t}(j) = \left(\frac{P_{i,t}(j)}{P_{i,t}}\right)^{-\epsilon_{\pi_i}} Y_{i,t}. \quad (26)$$

- Price Phillips curve for \mathcal{S}_1 :

$$\begin{aligned} & 1 - \pi_{1,t} \eta_{\pi_1} \left(\pi_{1,t} - \pi_{1,t-1}^{\iota_{\pi_1}} \right) \\ & + \beta \eta_{\pi_1} \mathbb{E}_t \left[\pi_{1,t+1} \frac{uc_{1,t+1}}{uc_{1,t}} \left(\pi_{1,t+1} - \pi_{1,t}^{\iota_{\pi_1}} \right) \frac{Y_{1,t+1}}{Y_{1,t}} \right] = \left(1 - \frac{1}{X_{1,t}} \right) \epsilon_{\pi_1}. \end{aligned} \quad (27)$$

- Price Phillips curve for \mathcal{S}_2 :

$$\begin{aligned} & 1 - \pi_{2,t} \eta_{\pi_2} \left(\pi_{2,t} - \pi_{2,t-1}^{\iota_{\pi_2}} \right) \\ & + \beta \eta_{\pi_2} \mathbb{E}_t \left[\pi_{2,t+1} \frac{uc_{1,t+1}}{uc_{1,t}} \left(\pi_{2,t+1} - \pi_{2,t}^{\iota_{\pi_2}} \right) \frac{Y_{2,t+1}}{Y_{2,t}} \right] = \left(1 - \frac{1}{X_{2,t}} \right) \epsilon_{\pi_2}. \end{aligned} \quad (28)$$

In the case of fully flexible prices ($\eta_{\pi} = 0$), the markup is set at its steady-state value $X_i = \frac{\epsilon_{\pi_i}}{\epsilon_{\pi_i} - 1}$. Retailers' profits are thus equal to:

$$\Pi_{r_1,t} = \left(1 - \frac{1}{X_{1,t}} \right) Y_{1,t} - \frac{\eta_{\pi_1}}{2} \left(\pi_{1,t} - \pi_{1,t-1}^{\iota_{\pi_1}} \right)^2 Y_{1,t}, \quad (29)$$

$$\Pi_{r_2,t} = \left(1 - \frac{1}{X_{2,t}} \right) Y_{2,t} - \frac{\eta_{\pi_2}}{2} \left(\pi_{2,t} - \pi_{2,t-1}^{\iota_{\pi_2}} \right)^2 Y_{2,t}. \quad (30)$$

Unions

Unions buy homogeneous labor services from households and differentiate them at no cost. Differentiated labor varieties are then aggregated back into CES aggregates by labor packers in homogeneous compounds, which are sold to the wholesale firm. The enforcement

of wage rigidities by means of labor unions is in line with [Smets and Wouters \(2007\)](#) and [Iacoviello and Neri \(2010\)](#), among others, and similarly to final goods price, it results from the presence of adjustment costs à la Rotemberg (with indexation parameter ι_w). Labor unions face the demand schedule $n_{i,t}(h) = \left(\frac{W_{i,t}(h)}{W_{i,t}}\right)^{-\epsilon_{w_i}} n_{i,t}$, $i = 1, 2$, from labor packers and maximize:

$$\mathbb{E}_0 \sum_{t=0}^{\infty} \beta^t \left\{ uc_{1,t} \left[\frac{W_{i,t}(h)}{P_{i,t}} n_{i,t}(h) - \frac{\eta_{w_i}}{2} \left(\frac{W_{i,t}(h)}{W_{i,t-1}(h)} - \pi_{i,t-1}^{\iota_w} \right)^2 \frac{W_{i,t}}{P_{i,t}} \right] - \frac{a_{\zeta,t} \phi_{i,t} n_{i,t}(h)^{1+\nu_i}}{1+\nu_i} \right\}. \quad (31)$$

Which gives the two wage Phillips curves:

- Wage Phillips curve for \mathcal{S}_1 :

$$\begin{aligned} \eta_{w_1} \omega_{1,t} \left(\omega_{1,t} - \pi_{1,t-1}^{\iota_{w_1}} \right) &= \beta \eta_{w_1} \mathbb{E}_t \frac{uc_{1,t+1}}{uc_{1,t}} \left(\omega_{1,t+1} - \pi_{1,t}^{\iota_{w_1}} \right) \frac{\omega_{1,t+1}^2}{\pi_{1,t+1}} \\ &+ (1 - \epsilon_{w_1}) n_{1,t} + \epsilon_{w_1} \left(\frac{\phi_{1,t} n_{1,t}^{1+\nu_1}}{w_{1,t} uc_{1,t}} \right). \end{aligned} \quad (32)$$

- Wage Phillips curve for \mathcal{S}_2 :

$$\begin{aligned} \eta_{w_2} \omega_{2,t} \left(\omega_{2,t} - \pi_{2,t-1}^{\iota_{w_2}} \right) &= \beta \eta_{w_2} \mathbb{E}_t \frac{uc_{1,t+1}}{uc_{1,t}} \left(\omega_{2,t+1} - \pi_{2,t}^{\iota_{w_2}} \right) \frac{\omega_{2,t+1}^2}{\pi_{2,t+1}} \\ &+ (1 - \epsilon_{w_2}) n_{2,t} + \epsilon_{w_2} \left(\frac{\phi_{2,t} n_{2,t}^{1+\nu_2}}{p_{2,t} w_{2,t} uc_{1,t}} \right). \end{aligned} \quad (33)$$

Above, $\omega_{1,t}$ and $\omega_{2,t}$ are nominal wage inflation, namely $\omega_{i,t} = \frac{W_{i,t}}{W_{i,t-1}} = \frac{P_{i,t} w_{i,t}}{P_{i,t-1} w_{i,t-1}} = \pi_{i,t} \frac{w_{i,t}}{w_{i,t-1}}$. Unions profits are therefore given by margins minus adjustment costs:

$$\Pi_{u_{1,t}} = \left(1 - \frac{1}{X_{w_{1,t}}} \right) w_{1,t} n_{1,t} - \frac{\eta_{w_1}}{2} \left(\omega_{1,t} - \pi_{1,t-1}^{\iota_{w_1}} \right)^2 w_{1,t} n_{1,t}, \quad (34)$$

$$\Pi_{u_{2,t}} = \left(1 - \frac{1}{X_{w_{2,t}}} \right) w_{2,t} n_{2,t} - \frac{\eta_{w_2}}{2} \left(\omega_{2,t} - \pi_{2,t-1}^{\iota_{w_2}} \right)^2 w_{2,t} n_{2,t}. \quad (35)$$

Monetary Policy

We assume that the central bank faces a ZLB constraint on the nominal interest rate r_t . This is particularly realistic in the context of the accommodating monetary policy reactions to the COVID-19 induced shocks. In order to combine the higher-order solution with the

occasionally binding ZLB, we assume that the central bank uses a barrier polynomial to constrain the gross nominal interest rate above unity:

$$R_t = c_0 + c_1 R_{unc,t} + c_2 R_{unc,t}^2. \quad (36)$$

The coefficients c_0 , c_1 and c_2 are obtained by fitting the polynomial to the ideal piecewise linear function:

$$R_t = \max \{1, R_{unc,t}\}. \quad (37)$$

The unconstrained interest rate $R_{unc,t}$ is set by the Taylor rule:

$$R_{unc,t} = R_{unc,t-1}^{r_R} R_{ss}^{1-r_R} \pi_t^{(1-r_R)r_\pi} \left(\frac{GDP_t}{GDP_{t-1}} \right)^{(1-r_R)r_Y} \left(\frac{\exp(\varepsilon_{e,t})}{a_{s,t}} \right). \quad (38)$$

In the Taylor rule (38), $a_{s,t}$ represents an autocorrelated term reflecting persistent shifts in the monetary policy desired target, while $\varepsilon_{e,t}$ captures momentary deviations.

The proposed approach to model the ZLB is motivated by the fact that, given that large shocks are considered, we want to preserve nonlinearity in the model solution within the two monetary policy regimes, instead of using a piecewise solution consisting of linear approximations inside each of the two regimes. Even if the correspondence between equation (36) and (37) will not be perfect, the additional smoothness of equation (36) with respect to (37) might also be regarded as a realistic feature of interest rate determination. This strategy is connected with the strand of the literature concerned with enforcing more complex occasionally binding constraints (as the ones on financial variables) by smooth perturbation solutions, like in [Dewachter and Wouters \(2014\)](#) and [Benigno et al. \(2020\)](#).

Aggregation and Equilibrium

The aggregate inflation rate is given by the weighted average of the inflation rates in the two sectors:

$$\pi_t = \pi_{1,t} \left(\frac{Y_{1,t}}{Y_{1,t} + p_{2,t} Y_{2,t}} \right) + \pi_{2,t} \left(\frac{p_{2,t} Y_{2,t}}{Y_{1,t} + p_{2,t} Y_{2,t}} \right). \quad (39)$$

Aggregate production is given by:

$$GDP_t = Y_{1,t} + p_{2,t} Y_{2,t}. \quad (40)$$

The evolution of the relative price of \mathcal{S}_2 is linked to the inflation rates in the two sectors:

$$\frac{p_{2,t}}{p_{2,t-1}} = \frac{\pi_{2,t}}{\pi_{1,t}}. \quad (41)$$

The model is closed with the resource constraints for the two goods, which also include all deadweight losses due to adjustment costs:

- Resource constraint for \mathcal{S}_1 :

$$\begin{aligned} c_{1,t} + k_{1,t} - (1 - \delta_{k_1}) k_{1,t-1} + p_{2,t} k_{2,t} + p_{2,t} (1 - \delta_{k_2}) k_{2,t-1} \\ = Y_{1,t} \left[1 - \frac{\eta_{\pi_1}}{2} \left(\pi_{1,t} - \pi_{1,t-1}^{\iota_{\pi_1}} \right)^2 \right] - \frac{\eta_{k_1}}{2} \left(\frac{k_{1,t}}{k_{1,t-1}} - 1 \right)^2 k_{1,t-1} \\ - p_{2,t} \frac{\eta_{k_2}}{2} \left(\frac{k_{2,t}}{k_{2,t-1}} - 1 \right)^2 k_{2,t-1} \\ - \frac{\eta_{w_1}}{2} \left(\omega_{1,t} - \pi_{1,t-1}^{\iota_{w_1}} \right)^2 w_{1,t} n_{1,t} - \Psi_{u_{1,t}} - p_{2,t} \Psi_{u_{2,t}}. \end{aligned} \quad (42)$$

- Resource constraint for \mathcal{S}_2 :

$$c_{2,t} = Y_{2,t} \left[1 - \frac{\eta_{\pi_2}}{2} \left(\pi_{2,t} - \pi_{2,t-1}^{\iota_{\pi_2}} \right)^2 \right] - \frac{\eta_{w_2}}{2} \left(\omega_{2,t} - \pi_{2,t-1}^{\iota_{w_2}} \right)^2 w_{2,t} n_{2,t}. \quad (43)$$

The two resource constraints (42) and (43) ensure that the amount of consumption, investment and adjustment costs are equal to production. Given that \mathcal{S}_2 is identified as the U.S. Leisure and Hospitality industry in the data, we postulate that investment goods are solely obtained out of \mathcal{S}_1 production.

By Walras's law, the model can be formulated either with the two resource constraints or with one resource constraint coupled with the household's budget constraint (2), producing the exactly equal results.

Exogenous Processes

The persistent exogenous processes are described by equations (44)-(50). The steady state of the intratemporal utility shock to \mathcal{S}_2 consumption, j^{ss} , the steady state of the labor supply shock to \mathcal{S}_1 , ϕ_1^{ss} , and the steady state of the labor supply shock to \mathcal{S}_2 , ϕ_2^{ss} are calibrated as to match the ratios of hours worked in the two sectors and the relative price of the two goods, precisely:

$$\log(a_{z_1,t}) = \rho_{z_1} \log(a_{z_1,t-1}) + \varepsilon_{z_1,t}, \quad (44)$$

$$\log(a_{z_2,t}) = \rho_{z_2} \log(a_{z_2,t-1}) + \varepsilon_{z_2,t}, \quad (45)$$

$$\log(a_{j,t}) = (1 - \rho_j) \log(j^{ss}) + \rho_j \log(a_{j,t-1}) + \varepsilon_{j,t}, \quad (46)$$

$$\log(a_{s,t}) = \rho_s \log(a_{s,t-1}) + \varepsilon_{s,t}, \quad (47)$$

$$\log(a_{\zeta,t}) = \rho_{\zeta} \log(a_{\zeta,t-1}) + \varepsilon_{\zeta,t}, \quad (48)$$

$$\log(\phi_{1,t}) = (1 - \rho_{\phi_1}) \log(\phi_1^{ss}) + \rho_{\phi_1} \log(\phi_{1,t-1}) + \varepsilon_{\phi_1,t}, \quad (49)$$

$$\log(\phi_{2,t}) = (1 - \rho_{\phi_2}) \log(\phi_2^{ss}) + \rho_{\phi_2} \log(\phi_{2,t-1}) + \varepsilon_{\phi_2,t}. \quad (50)$$

The standard deviations of the innovations appearing in equations (44)-(50) and the uncorrelated shock to the monetary policy target $\varepsilon_{e,t}$, are denoted by:

$$\boldsymbol{\sigma} = [\sigma_{z_1}, \sigma_{z_2}, \sigma_j, \sigma_s, \sigma_{\zeta}, \sigma_{\phi_1}, \sigma_{\phi_2}, \sigma_{e,t}]'. \quad (51)$$

3 Large Shocks and Model Solution

The model described in Section 2 enlarged with large shocks and ZLB becomes a nonlinear, non-Gaussian model. Subsection 3.1 introduces the large shock into the model, and Subsection 3.2 discusses model solution and nonlinearity.

3.1 Non-Gaussianity

The model outlined in Section 2 represents a nonlinear system of rational expectations, which is driven by the following vector of structural shocks:

$$\boldsymbol{\varepsilon}_t = [\varepsilon_{z_1,t}, \varepsilon_{z_2,t}, \varepsilon_{j,t}, \varepsilon_{\zeta,t}, \varepsilon_{\phi_1,t}, \varepsilon_{\phi_2,t}, \varepsilon_{s,t}, \varepsilon_{e,t}]'. \quad (52)$$

We allow the first six innovations to (possibly) display large shocks. To exclude wild movements in the policy rate, which are unrelated to movements in prices and real activity, we do not allow large shocks to the two monetary policy innovations, namely $\varepsilon_{s,t}$ (the one related with persistent central bank deviations from the target) and $\varepsilon_{e,t}$ (the one related with temporary ones).

Modelling large shocks is a challenging task, in that the rarity of the involved events pre-

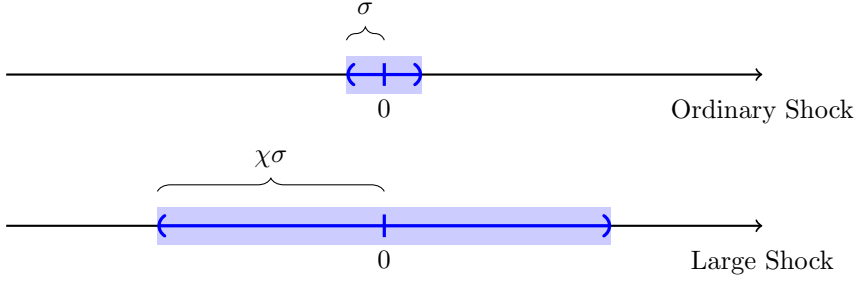


Figure 2: The modelization of large shocks. The upper panel reports the ordinary shock centered at 0 and with a standard deviation equal to σ . The bottom panel reports the large shock with an inflated standard deviation equal to $\chi \cdot \sigma$. The factor of increase in variability is calibrated to $\chi = 10$.

cludes us from observing a numerous enough sample to estimate their characteristics. Our strategy is then to be agnostic and to accommodate the possibility of very diverse scenarios. In particular, we assume that the aforementioned six shocks can be drawn from (i) the ordinary component, consisting in a zero-mean normal with ordinary standard deviation σ_i (ii) the large shock component, consisting in a normal with an inflated standard deviation equal to $\chi \cdot \sigma_i$. A graphical representation is provided in Figure 2. The large shock parameter χ is calibrated as to provide sensible ranges for the magnitude of the shocks responsible for the pandemic-related disruption. In particular, the calibrated factor of the increase in variability χ guarantees that the large shock may realize in a wide interval, and that large favorable rebounds resulting from economy re-openings are allowed. Based on simulations (available upon request), we found it plausible that the large shocks could live somewhere in the interval between minus thirty to thirty times the ordinary standard deviations, which amounts to selecting $\chi = 10$.

A second source of difficulty is the specification of the dependencies between the various disaster components. Ideally, the filter should be able to distinguish between cases in which the large shock arises either from just one component, some combination of them or all of them. Defining \mathcal{D} the set of shocks that may display rare disasters, the possible components of the mixture are represented by the elements in the power set $\mathcal{S} = \mathcal{P}(\mathcal{D})$. The standardized shocks $\left(\tilde{\varepsilon}_t = \frac{\varepsilon_t}{\sigma}\right)$ are then distributed according to the following mixture of Gaussians:

$$p(\tilde{\varepsilon}_t) = \left(1 - \sum_{k=1}^K \psi_{k,t}\right) \mathcal{N}(0, I) + \sum_{k=1}^K \psi_{k,t} \mathcal{N}(0, \Omega_k), \quad (53)$$

where: K is the number of components; $\psi_{k,t}$ is the k -th probability at time t ; and Ω_k is a diagonal covariance matrix where each element is one (χ^2) in correspondence with shocks

that are ordinary (large) in the k -th component.

We assume *a priori*, equiprobability for all the sixty-three disasters combinations, precisely, $\psi_{k,t} = \psi_t/63$. In this paper we do not fix the time-varying disaster probabilities (ψ_t), but they are estimated together with the DSGE parameters, see Section 5.

It is worth noting that our large shocks modeling is similar to [Lenza and Primiceri \(2020\)](#). They show that, by allowing for an inflating factor of the variance of the VAR shocks in the pandemic quarters, it is possible to use these last data meaningfully and to improve on the precision of forecasts with respect to the strategy of just discarding them. In their work, the inflating factor is estimated, while its occurrence is fixed in the months of the pandemic. Conversely, in this paper, the entity of large shocks is calibrated (even if in a diffuse way), while the occurrence of the disaster is estimated by the filter. Moreover, unlike [Lenza and Primiceri \(2020\)](#), we do not assume that all the shocks are subject to a magnified variability, but we leave the door open for an increase in the variance of just some of them.

3.2 Nonlinearity

To account for higher-order effects in the transmission of large shocks and the ZLB, the model decision rules are approximated nonlinearly. Indeed, a first-order approximation would neglect the interaction terms in the transmission of shocks, an undesirable feature in our large shock framework. Differently, a nonlinear approximation enables us to consider the differentiated state-dependent responses of the economy to large shocks. Secondly, the smooth ZLB described in Section 2 would be completely missed by a linear approximation, as visible in Figure 3.

To estimate the model in a reasonable amount of time, a fast solution method is needed, therefore we follow [Levintal \(2017\)](#) and use a second-order perturbation. The solution is computed around the non-stochastic steady state, which is derived in Appendix 7.

The perturbation solution depends on the moments of the shocks, and we assume that the shocks are always coming from the ordinary component. This is equivalent to postulating that the pandemic shocks are completely unexpected by the agents of the model who do not anticipate the possibility of large shocks and do not operate any uncertainty correction regarding them.

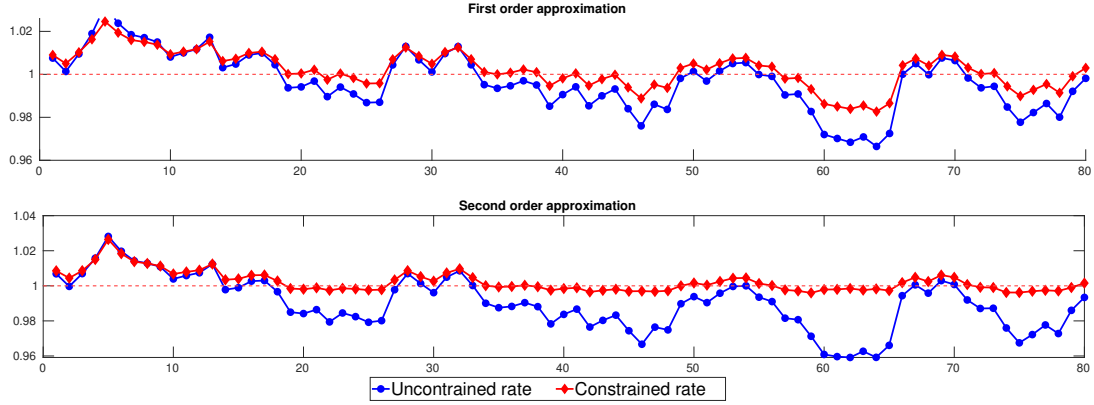


Figure 3: First and second order approximation. The figure reports a simulation of the unconstrained and constrained interest rates using the smooth barrier polynomial, see Section 2, at the first and second order, for a given sequence of shocks. The blue (circle) line is the unconstrained interest rate, while the red (diamond) line is constrained rate. In the first order approximation the constrained rate would be allowed to substantially cross the lower bound, whereas in the second order approximation it is effectively constrained.

The model solution gives:

$$\begin{aligned} x_t^C &= g(x_t^S; \theta), \\ x_{t+1}^S &= h(x_t^S; \theta) + R(\theta) \tilde{\varepsilon}_{t+1}, \end{aligned} \quad (54)$$

where: s_t^S are the model states; s_t^C are the model controls; R is the matrix that links the standardized shocks to the model states; and θ is the parameters vector. The nonlinearity arises from $g(\cdot)$ and $h(\cdot)$ being second order polynomials in the economic states.

The model variables are linked to their observable data counterpart through the measurement equations:

$$\mathbf{y}_t = A + B\mathbf{x}_t + u_t, \quad u_t \sim \mathcal{N}(0, H), \quad (55)$$

where: \mathbf{y}_t are the observed series; $\mathbf{x}_t = \begin{bmatrix} x_t^S \\ x_t^C \end{bmatrix}'$ is the stacked vector of economic states and controls; and u_t are the measurement errors.

As we will discuss in Section 6, we consider eleven series, since the number of structural shocks is eight, adding measurement errors is necessary to avoid stochastic singularity, see [Herbst and Schorfheide \(2015\)](#). We assume that H is diagonal and that it has a standard deviation equal to 15% of the variability of the corresponding data series. We exclude the pandemic quarters to avoid over-inflating the measurement error variance.

4 Filtering the Nonlinear DSGE with disaster shocks

For any combination of model parameters θ , the state-space representation described in equations (54) and (55) implicitly defines the transition and measurement densities $p(\mathbf{x}_t|\mathbf{x}_{t-1};\theta)$ and $p(\mathbf{y}_t|\mathbf{x}_t;\theta)$, from which the joint distribution of unobserved states and observations can be constructed:

$$p(\mathbf{x}_{1:T}, \mathbf{y}_{1:T}|\theta) = \prod_{t=1}^T p(\mathbf{x}_t|\mathbf{x}_{t-1};\theta) p(\mathbf{y}_t|\mathbf{x}_t;\theta). \quad (56)$$

By recursively integrating the unobserved states from the joint density in (56), the likelihood function can be computed by prediction error decomposition:

$$p(\mathbf{y}_{1:T}|\theta) = \prod_{t=1}^T p(\mathbf{y}_t|\mathbf{y}_{1:t-1};\theta). \quad (57)$$

In non-Gaussian nonlinear state-space models, the densities appearing in the equations (56) and (57) do not have closed-form solutions and simulation methods, such as PFs, have to be used. Since the seminal paper of [Gordon et al. \(1993\)](#), PFs have been used in non-linearized DSGE models; see [An and Schorfheide \(2007\)](#), [Fernández-Villaverde and Rubio-Ramírez \(2007\)](#), [Fernández-Villaverde et al. \(2011\)](#) and [Flury and Shephard \(2011\)](#). Unfortunately, PFs suffer from the curse of dimensionality as they require an exponentially increasing number of particles, see [Bengtsson et al. \(2008\)](#). For this reason, PFs entail a high computational burden even for medium-sized models such as ours. To overcome this issue, different solutions have been proposed. Among them, [Liu and Chen \(1998\)](#) propose the Conditionally Optimal Particle Filter (COPF), whose effectiveness in the context of DSGE estimation has been shown by [Herbst and Schorfheide \(2015\)](#) and [Aruoba et al. \(2021\)](#). Unfortunately, except for special cases, closed-form expressions for the conditionally optimal density used by the COPF is difficult to derive or not available. In those cases, a possible alternative is the Approximate Conditionally Optimal Particle Filter (ACOPF), namely a PF that uses an approximation to the unknown optimal proposal density and is derived in Appendix D.

The presence of large shocks (economic disasters) represents an additional blow to the effectiveness of PFs. Large shocks require an enormous number of particles to describe all possible outcomes which may occur after a disaster, see [Pitt and Shephard \(1999\)](#) and

Amisano and Tristani (2011). The problem associated with outliers in the observations has also been stressed by Herbst and Schorfheide (2015) who show that the data related to the Great Recession challenge the effectiveness of PFs in estimating DSGE models. In this respect, it is worth noticing that COVID-19 created “swings” in the time-series that had never been seen before and that were much larger than the 2008-09 crisis.

Unlike the SMC filters, the Sigma points filters (SPF) assume a convenient parametric form for the densities appearing in the Bayesian filtering recursion and replace the particles of simulation-based methods with a small set of (deterministically) chosen points that are used to compute, recursively, the moments of the densities. A textbook treatment of the of Gaussian filters can be found in Särkkä (2013). They also have been applied to estimate nonlinear DSGE, see among others Andreasen (2012, 2013), Ivashchenko (2014), Kollmann (2015), Binning and Maih (2015), Noh (2019) and Benigno et al. (2020). While these filters are approximate by construction, Andreasen (2013) and Kollmann (2015) show that they can outperform prohibitively burdensome PFs.

5 Mixture of Mixture of Cubature Kalman Filter

To deal with the nonlinear and non-Gaussian state-space with (possibly) large shocks, we propose a new filter that is a Mixture of Mixture of Cubature Kalman Filter (MM-CKF), which tests all the possible disaster shocks (large deviation in state noise) realization and easily handles nonlinearity at the same time. The filter also gives the approximated likelihood in a fraction of the time employed by the PFs.

GSF, also known as Gaussian Mixture Filters, have been initially introduced in the signal processing literature by Sorenson and Alspach (1971) and Alspach and Sorenson (1972). These filters represent the posterior densities of unobserved states as mixtures of normals:

$$p(\mathbf{x}_t | \mathbf{y}_{1:t}) \approx \sum_{n=1}^{G_t} p(\mathbf{x}_t | \kappa_t^n, \mathbf{y}_{1:t}) p(\kappa_t^n | \mathbf{y}_{1:t}) = \sum_{n=1}^{G_t} \mathcal{N}(m_{t|t}^n, P_{t|t}^n) w_{t|t}^n, \quad (58)$$

where G_t are the number of the mixture components, κ_t^n is an indicator variable and $w_{t|t}^n$ are the corresponding weights at time t . GSF share the idea that any probability density arising from e.g. nonlinearity, can be approximated with arbitrary precision by a

weighted sum of Gaussian densities (Alspach and Sorenson, 1972). The first two moments $m_{t|t}^n$ and $P_{t|t}^n$ of each component are recursively estimated by banks of filters running in parallel. Banks of Kalman filters, Extended Kalman filters, Particle filters, Unscented Kalman filters, Cubature Kalman filters have been used by Sorenson and Alspach (1971), Alspach and Sorenson (1972), Kotecha and Djuric (2003), Faubel et al. (2009) and Leong et al. (2013).

In our model, the disaster shocks will over-inflate the state equation variance. To deal with the nonlinearity and the non-Gaussianity, we split each prediction density (G_t) that handles nonlinearity into as many components as the ones making up the noise mixture $p(\tilde{\boldsymbol{\varepsilon}}_t) = \sum_{k=1}^K \psi_k p(\boldsymbol{\varepsilon}_t^k)$ described in equation (53). Equation (58) becomes:

$$\begin{aligned} p(\mathbf{x}_{t+1}|\mathbf{y}_{1:t}) &\approx \sum_{n=1}^{G_t} \sum_{k=1}^K p\left(\mathbf{x}_{t+1}|\kappa_{t+1}^{(n,k)}, \mathbf{y}_{1:t}\right) p\left(\kappa_{t+1}^{(n,k)}|\mathbf{y}_{1:t}\right) \\ &= \sum_{n=1}^{G_t} \sum_{k=1}^K \mathcal{N}\left(m_{t+1|t}^{(n,k)}, P_{t+1|t}^{(n,k)}\right) w_{t+1|t}^{n,k}, \end{aligned} \tag{59}$$

where $w_{t|t}^{n,k}$ stands for $w_{t|t}^n \psi_t^k$. The splitting stage of the filter is followed by a merging one. Indeed, given that for each of the G_t components, K new filters are created, an exponentially increasing number of densities would arise. In this regard, we opt for a collapsing strategy that constantly retains G_t components in each iteration t . Unlike Faubel et al. (2009) and Leong et al. (2013), we use a collapsing procedure that keeps the G_t mixands with the largest weights as suggested by Kotecha and Djuric (2003) in the context of a GSPF. Moreover, we can fix G_t to be constant, and in the case of $G_t = 1$, the nonlinearity is just handled by the CKF and the non-Gaussianity (mixture) in the state is estimated using the K new filters created. Finally if $G_t = 1$ and $K = 1$, the filter collapses to the well-known CKF.

A sketch of the MM-CKF is provided below (Algorithm 1), a detailed description is reported in Appendix B.

Algorithm 1 Sketch of the MM-CKF filter.

for $t = 1$ to T **do**

The filtering density of unobserved states is approximated by $p(\mathbf{x}_{t-1}|\mathbf{y}_{1:t-1}) = \sum_{n=1}^{G_{t-1}} \mathcal{N}\left(m_{t-1|t-1}^n, P_{t-1|t-1}^n\right) w_{t-1|t-1}^n$.

for $g = 1$ to G_{t-1} **do**

for $k = 1$ to K **do**

Use the **CKF** to update mean $m_{t|t}^{n,k}$, variance $P_{t|t}^{n,k}$ and weight $w_{t|t}^{n,k}$ of the $\{g^{th}, k^{th}\}$ mixand, assuming noise is coming from the k^{th} component.

end for

end for

Reduce the number of mixands if $G_{t-1}K > \bar{G}$ or if some weight is negligible.

end for

In Algorithm 1, the last period filtered unobserved components:

$$p(\mathbf{x}_{t-1}|\mathbf{y}_{1:t-1}) = \sum_{n=1}^{G_{t-1}} \mathcal{N}\left(m_{t-1|t-1}^n, P_{t-1|t-1}^n\right) w_{t-1|t-1}^n,$$

make predictions on the unobserved states. For each of the G_{t-1} filtered components forming the filtered density and for each of the K components forming the state noise, the algorithm uses the CKF formulae to compute the predicted mean $\mu_{t|t-1}^{n,k}$ and the covariance $P_{t|t-1}^{n,k}$ for the unobserved states supposing noise is coming from k^{th} component.

The density of predicted unobserved states, for each shock combination, is then approximated by:

$$p\left(\mathbf{x}_t|\mathbf{y}_{1:t-1}, \kappa_t^{n,k}\right) = \mathcal{N}\left(\mu_{t|t-1}^{n,k}, P_{t|t-1}^{n,k}\right), \quad n = 1, \dots, G_t, \quad k = 1, \dots, K.$$

The predicted unobserved states are approximated by the ensemble density:

$$p(\mathbf{x}_t|\mathbf{y}_{1:t-1}) = \sum_{n=1}^{G_{t-1}} \sum_{k=1}^K \mathcal{N}\left(\mu_{t|t-1}^{n,k}, P_{t|t-1}^{n,k}\right) w_{t|t-1}^{n,k},$$

where the predicted weights for each component are given by $w_{t|t-1}^{n,k} = w_{t-1|t-1}^n \psi_k$, for $k = 1, \dots, K$.

For each of the $G_{t-1}K$ predicted components, use the CKF formulae to compute the

predicted observations mean $\mathcal{Y}_{t|t-1}^{n,k}$, the predicted observations covariance $\mathcal{F}_{t|t-1}^{n,k}$ and the predicted variance-covariance between unobserved states and observations $\mathcal{P}_{t|t-1}^{n,k,\mathbf{xy}}$. With these quantities, the CKF updating is performed using the new observation \mathbf{y}_t in order to obtain the new filtered means $\mu_{t|t}^{n,k}$ and covariances $P_{t|t}^{n,k}$ for unobserved states. Weights are then updated using the Bayes' rule:

$$w_{t|t}^{n,k} = \frac{w_{t|t-1}^{n,k} \mathcal{N}(\mathbf{y}_t; \mathcal{Y}_{t|t-1}^{n,k}, \mathcal{F}_{t|t-1}^{n,k})}{\sum_{n=1}^{G_{t-1}} \sum_{k=1}^K w_{t|t-1}^{n,k} \mathcal{N}(\mathbf{y}_t; \mathcal{Y}_{t|t-1}^{n,k}, \mathcal{F}_{t|t-1}^{n,k})}.$$

To avoid incurring an exponential proliferation of the number of components, a collapsing strategy for the number of mixands is performed, as detailed in Appendix B. More specifically, components with negligible weights are removed from the mixture and if the number of components exceeds the maximum of G_t , than the most significant ones are retained. Upon computing these quantities, a new iteration of the filter can be run.

Our approach to non-Gaussianity is drawn from the engineering literature where a similar decomposition is used for nonlinear state estimation see, among others, [Pei et al. \(2013\)](#) and [Pei et al. \(2014\)](#). Splitting rules based on Gaussian mixtures to treat large measurement errors or system noise has been employed in disparate branches of the signal processing. In our specific case, the different components of the system noise stem from the various possible large economic shocks to be tested. The splitting rule is indeed the direct translation, in the CKF framework, of the ones presented in [Alspach and Sorenson \(1972\)](#) for KFs and [Kotecha and Djuric \(2003\)](#) for PFs.

Splitting the filter into the K mixture components at each time t is a computationally costly operation to be repeated throughout the millions of likelihood evaluations required by the SMC. To speed up the computational times, we avoid splitting the filter when it is irrelevant. Indeed, a simple plot of the time series suggests that it is very unlikely to observe disaster shocks (e.g. COVID-19 type shocks) before 2020. At the same time, we do not want to completely exclude the possibility of detecting large shocks before the pandemic quarters. The filter, by construction, does not split when the estimated ex-ante probability of large shock ψ_t is too low (namely, $\psi_t < \bar{\psi} = 10^{-3}$). We have to stress that ψ_t is estimated endogenously together with the DSGE parameters and not fixed a priori. As a robustness check, we use an always-splitting version of the filter on the estimated

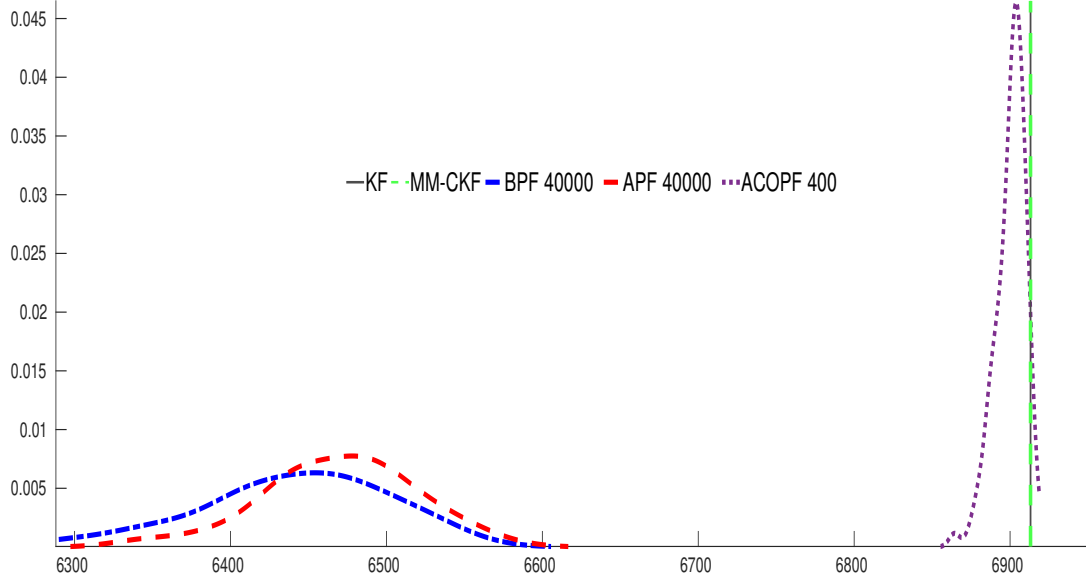


Figure 4: Monte Carlo results for $N = 100$ log-likelihood evaluation. The considered filters are the Kalman Filter (KF), the Bootstrap Particle filter (BPF), the Auxiliary particle filter (APF), the Conditionally Optimal Particle Filter (COPF) and the Mixture of Mixture Cubature Kalman Filter (MM-CKF). The vertical reports the results for the deterministic KF (black vertical) and the MM-CKF (green dotted vertical line). The BPF (blue dashed-dot), APF (red dashed) and COPF (purple dotted) have negative bias.

parameters to verify that no disaster shock is actually detected before 2020. Results are available from the authors upon request. To show that our filter can correctly identify the source of the shock and outperform asymptotically PFs with a massively reduced running time (see also [Andreasen, 2013](#) and [Kollmann, 2015](#)) we run three simulation experiments. In the first experiment, we simulate $N = 100$ times the model described in Section 2 and we apply a first order approximation, bringing to a linear and Gaussian model. In this case the KF is the optimal filter and gives the exact likelihood. Figure 4 reports the Monte Carlo results and shows that MM-CKF collapses to the KF while the BPF, the APF, and the COPF have bias likelihood.

In the second experiment we simulate $N = 100$ times the model in Section 2, we take a second-order approximation and finally add a random large (state) shock. The resulting model is nonlinear and non-Gaussian and the exact expression for the likelihood is not available. To compare the performances of MM-CKF with the other filters, we use the RMSE of the filtered and the (true) latent state:

$$RMSE_{i,f} = \sqrt{\frac{1}{N} \sum_{j=1}^N \sum_{t=1}^T \left(\hat{\mathbf{x}}_{i,t|t}^f - \mathbf{x}_{i,t} \right)^2}.$$

where $\hat{\mathbf{x}}_{i,t}^f$ for $i = 1, \dots, n$ and $\mathbf{x}_{i,t}$ for $i = 1, \dots, n$ are the filtered simulated latent states. Table 1 reports a selection of the RMSE (full table is in Appendix E) and the computing time (in seconds) for the KF, BPF with 40000 particles, APF with 40000 particle, COPF with 400 and 4000 particles and the MM-CKF with $G_t \leq 4$.

Table 1 shows that the MM-CKF is much faster than the BPF, APF and the ACOPF. The KF, clearly, is the fastest filter but gives biased results. Overall, the results show that the MM-CKF is a valuable choice in filtering unknown latent states when computational time and robustness to large shocks are crucial. In the third Monte Carlo experiment, we

Table 1: RMSE of the Monte Carlo experiment for $N = 100$ replications of the Two-Sector model with large shocks. The Table reports the full name (Full Name) with the associated symbol (Symbol). The filters are: Kalman filter (KF); Bootstrap Particle Filter with 40000 particles (BPF); Auxiliary Particle Filter with 40000 particles (APF); the Approximate Optimal Particle Filter with 400 and 4000 particles (ACOPF(400), ACOPF(4000)); and the Mixture of Mixture of Cubature Kalman Filter (MM-CKF) with four components ($G_t = 4$).

Full Name	Symbol	KF	BPF	APF	ACOPF(400)	ACOPF(4000)	MM-CKF
Hours \mathcal{S}_1	n_1	0.33	0.53	0.54	0.25	0.20	0.16
Hours \mathcal{S}_2	n_2	0.05	0.07	0.07	0.04	0.03	0.02
Production \mathcal{S}_1	Y_1	1.20	2.00	2.00	1.30	0.77	0.59
Production \mathcal{S}_2	Y_2	0.23	0.34	0.33	0.23	0.15	0.14
Consumption \mathcal{S}_1	c_1	0.79	1.60	1.60	0.95	0.56	0.47
Consumption \mathcal{S}_2	c_2	0.23	0.34	0.33	0.23	0.15	0.14
Capital \mathcal{S}_1	k_1	16.00	16.00	14.00	10.00	6.90	6.00
Capital \mathcal{S}_2	k_2	2.20	2.90	2.90	2.10	1.60	1.30
Relative price	p_2	0.83	1.10	1.00	0.74	0.55	0.47
Inflation	π	0.05	0.08	0.07	0.01	0.01	0.00

<i>Time in Seconds</i>						
KF	BPF	APF	ACOPF(400)	ACOPF(4000)	MM-CKF	
0.09	650.00	1200.00	870.00	4800.00	1.20	

study whether the MM-CKF provides a good identification of large shocks. We simulate $N = 500$ times the model of Section 2 with the parameters obtained from our empirical application, see Section 6. We then add negative (i.e. Realized Disaster) and then positive (i.e. Realized Rebound) shocks of the same type and intensity found in our empirical application. To closely match the real data, the length of the simulated series is equal to $T = 142$, the realized disaster is simulated at $t = 131$ and the realized rebound at $t = 132$. Table 2 reports the Monte Carlo results. The MM-CKF rightly detects large shocks type and time location. More precisely considering $T = 142$ and $N = 500$ we have 71000 data points where normal observations, realized disaster and realized rebound can occur. By

design, we have 70000 normal observations, 500 realized disaster and 500 realized rebound, that occur sequentially. Finally, from our model, we have $K = 64$ possible combinations of large shocks. As the Table shows, the MM-CKF correctly selects the ordinary shocks 97% of the time, the location and combination of the disaster shock 90% of the time, the location and combination of the rebound 86% of the time and, finally, the location and combination of both 81% of the time.

Table 2 results are also analyzed in Figure 5. The figure shows the likelihood for a small subset of the $K = 64$ (possible) large shocks components, by zooming around the disaster and rebound events. The likelihood of the four components are: the ordinary component (the one without large shocks); the component number two in the shock mixture (the one with only a large shock to labor supply in \mathcal{S}_1); the component which, according to our empirical application, realizes in the disaster period $t = 131$; and the component which, accordingly to our empirical application, realizes in the rebound period $t = 132$. As the Figure shows, the ordinary component (blue line) is the one with the largest log-likelihood before and after the disaster periods, while in such quarters the disaster and rebound components are correctly identified, with the highest log-likelihood of the realized disaster (red squared line) at $t = 131$ and the highest log-likelihood of the realized rebound (black circle line) at $t = 132$.

We conclude this experiment with Figure 6 that provides a closer look at the disaster and rebound quarters, showing the log-likelihood of each of the possible $K = 64$ combinations at time $T = 131$ and $T = 132$. The realized disaster and rebound combinations are recognized as the ones with the highest log-likelihood among the other combinations. The figure also reports the log-likelihood ratio for realized disaster and rebound, showing that one combination has the highest weight, while the others have small or null weights.

6 Empirical Analysis

6.1 Data

We estimate the model on US quarterly data from 1985:Q1 to 2020:Q3. Eleven model variables are linked to the data series: value-added in the general sector; value-added in the Leisure and Hospitality sector; aggregate investment; aggregate consumption; hours worked in the general sector; hours worked in the Leisure and Hospitality sector; price

Table 2: Shock type and location Monte Carlo results for $T = 142$ and $N = 500$ replications. The table reports: the shock type (Shock type); the number of times it is present in the simulated dataset (Occurred); the number of times it is detected (Detected); and the results in percentage (Percentage). The possible outcome of the experiment are: normal observations (Ordinary), realized disaster (Disaster); realized rebound (Rebound), and realized disaster and rebound that occur sequentially (Both).

Shock type	Occurred	Detected	Percentage
Ordinary	70000	68221	97%
Disaster	500	450	90%
Rebound	500	430	86%
Both	500	405	81%

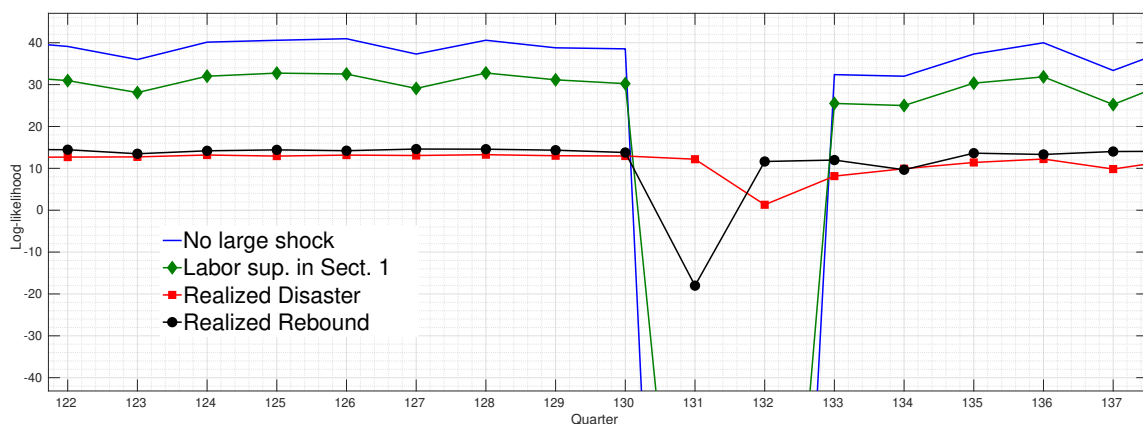


Figure 5: The Figure reports the log-likelihood of four components: the ordinary component (No large shock, blue continuous line); the component number two among the $K = 64$ possible outcome corresponding to a large shock to labor supply in S_1 (Labor supply shock in Section 1, green diamond line); the component corresponding to the simulated realized disaster at time $t = 131$ (Realized Disaster, red squared line); the component corresponding to the simulated realized rebound at time $t = 132$ (Realized Rebound, black circle line).

inflation in the general sector; price inflation in the Leisure and Hospitality sector; wage inflation in the general sector; wage inflation in the Leisure and Hospitality sector; and the Federal Funds Rate. Value-added, investment, consumption and hours are taken in per capita terms and in demeaned growth rates; price and wage inflation are demeaned; the Federal Funds Rate is in level. A detailed description regarding the sources and the construction of the data is provided in Appendix A. The sectoral value-added and inflation, which is retrieved from the BEA, are available at annual frequencies before 2005 and quarterly frequencies thereafter. To this end, we let these data be handled as missing by the MM-CKF, which removes the corresponding columns for the missing quarters in the Cubature Kalman gain matrix.

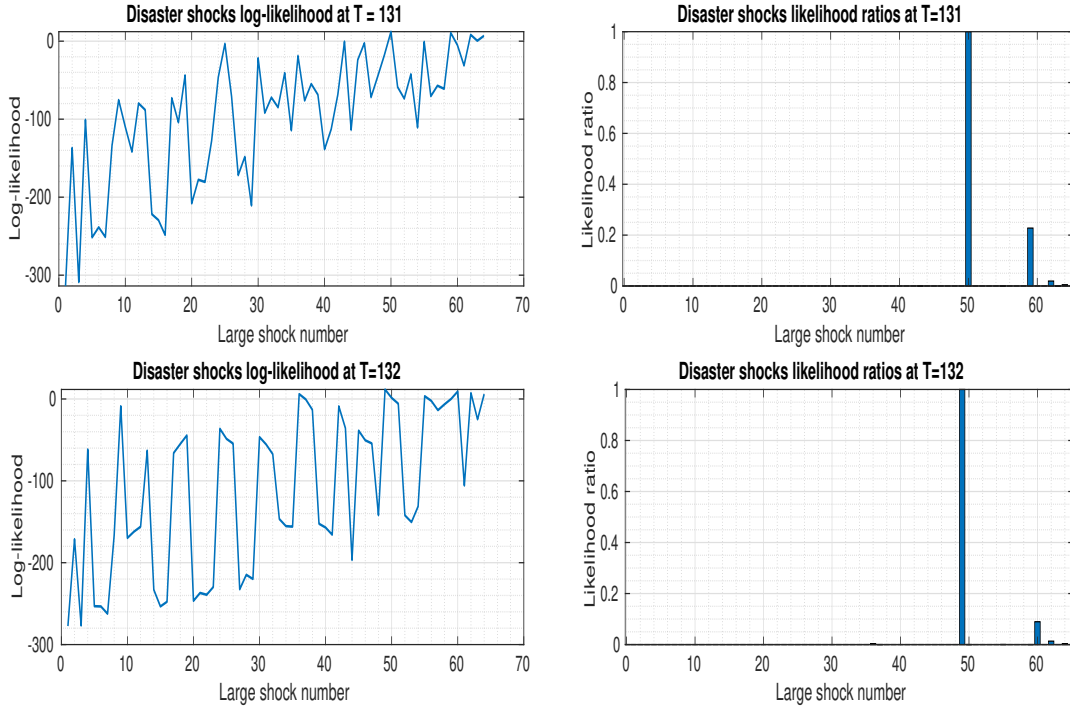


Figure 6: Log-likelihood and likelihood ratio for each of the possible $K = 64$ combinations at realized disaster ($T = 131$, upper plots) and realized rebound ($T = 132$, lower plots). The left plots report the log-likelihood for all the $K = 64$ possible combinations in the realized disaster (upper left plot) and realized rebound (lower left plot). The right upper plot reports the ratio of the highest component with respect to the remaining in for the disaster shock. The right lower plot reports the ratio of the highest component with respect to the remaining in for the rebound shock.

6.2 Prior Specification

Following [Del Negro and Schorfheide \(2008\)](#), we partition the model parameters into three categories: parameters determining the steady state ($\Theta_{(ss)}$); parameters related to the endogenous propagation mechanism ($\Theta_{(endo)}$); and parameters associated with the law of motion of the exogenous variables ($\Theta_{(exo)}$):

$$\begin{aligned}
 \Theta_{(ss)} &= [\beta, \alpha_1, \alpha_2, \delta_{k_1}, \delta_{k_2}, \epsilon_{\pi_1}, \epsilon_{\pi_2}, \epsilon_{w_1}, \epsilon_{w_2}, j^{ss}, \phi_1^{ss}, \phi_2^{ss}, \nu_1, \nu_2]', \\
 \Theta_{(endo)} &= [r_R, r_Y, r_\pi, \iota_{\pi_1}, \iota_{\pi_2}, \iota_{w_1}, \iota_{w_2}, h_1, h_2, \eta_{\pi_1}, \eta_{\pi_2}, \eta_{w_1}, \eta_{w_2}, \eta_{u_1}, \\
 &\quad \eta_{u_2}, \eta_{k_1}, \eta_{k_2}]', \\
 \Theta_{(exo)} &= [\rho_{z_1}, \rho_{z_2}, \rho_j, \rho_{\phi_1}, \rho_{\phi_2}, \rho_\zeta, \rho_s, \sigma_{z_1}, \sigma_{z_2}, \sigma_j, \sigma_{\phi_1}, \sigma_{\phi_2}, \sigma_\zeta, \sigma_s, \sigma_e]'.
 \end{aligned} \tag{60}$$

For the price and wage stickiness parameters, we specify the priors in terms of the Calvo-related parameter θ_i , $i \in \{\pi_1, \pi_2, w_1, w_2\}$, which can be linked to η_i according to:

$$\eta_i = \frac{\theta_i(\epsilon_i - 1)}{(\beta\theta_i - 1)(\theta_i - 1)}.$$

We calibrate the parameters belonging to $\Theta_{(ss)}$ basing on “gross ratios” and historical averages. We set $\beta = 0.991$ to obtain a real annual interest rate of 3 percent at the steady-state. The elasticity of substitution for the two final goods and for the labor varieties is set equal to $\epsilon_{\pi_1} = \epsilon_{\pi_2} = \epsilon_{w_1} = \epsilon_{w_2} = 1/0.15 + 1$ in order to imply steady state markups of 15 percent. The quarterly capital depreciation rates are set to $\delta_{k_1} = \delta_{k_2} = 0.025$, to induce a steady-state investment to output ratio of 22 percent. Capital share parameters in technology are fixed equal to $\alpha_1 = \alpha_2 = 0.35$, in order to match a labor share of income of 65 percent. The labor disutility curvature parameters ν_1 and ν_2 , which prove to be hardly estimated, are calibrated to 0.5, following standard macro calibration. We normalize the hours worked in sector \mathcal{S}_1 as $n_1 = 1$ and set the steady-state of hours worked in sector \mathcal{S}_2 as $n_2 = 0.07$, to reflect the mean ratio of the hours worked in the two sectors observed in the sample. We also target the mean relative price between sector \mathcal{S}_2 and the rest of the economy by imposing $p_2 = 0.78$ at the steady-state. The above steady-state conditions jointly imply $j^{ss} = 0.0715$, $\phi_1^{ss} = 0.643$ and $\phi_2^{ss} = 1.896$. Details on the steady-state derivations are provided in Appendix B. In addition to the steady-state parameters, as in [Iacoviello and Neri \(2010\)](#), we also fix the autocorrelation of the persistent monetary policy shock $\rho_s = 0.975$. In the present baseline estimation exercise, in order to facilitate convergence, we assume no indexation $\iota_{\pi_1} = \iota_{\pi_2} = \iota_{w_1} = \iota_{w_2} = 0$ and we also fix the autocorrelation of labor supply shocks in sector \mathcal{S}_2 . Based on pre-sample estimates, one parameter appeared to be weakly identified ($\rho_{\phi_2} = 0.84$). Data also seems to be quite silent about the sectoral differences of parameters related to consumption and investment. This is no surprise, considering that, for consumption and investment, we only dispose of aggregate series. We then estimate the parameters governing habits, capital adjustment and capital utilization under the restriction of being the same in the two sectors (namely, $h_1 = h_2$, $\eta_{k_1} = \eta_{k_2}$ and $\eta_{u,1} = \eta_{u,2}$). Overall, the number of estimated parameters is 23, while the calibrated ones are 20.

For the sake of comparability to other studies, the priors are formed based on the ones of

Smets and Wouters (2007). Priors are summarized in Table 3, along with posterior results. The priors reflect estimates of moderate habits in consumption, of moderate price and wage rigidities in sectors \mathcal{S}_1 and \mathcal{S}_2 , substantial monetary policy inertia, moderate concern for output stabilization and a strong one for the inflation level. For the autoregressive coefficients, the priors are loosely centered around 0.50, to allow the sampler to potentially distinguish between exogenous persistence mechanisms and endogenous ones, a point made by Herbst and Schorfheide (2014).

6.3 Inference Strategy

The estimation is carried out using the SMC sampler that has already been used in the DSGE literature by Creal (2007) and Herbst and Schorfheide (2014, 2015). We refer to the above papers for a detailed description of the procedure. The SMC requires a likelihood tempering approach, which targets a sequence of tempered posterior densities $[p(\mathbf{y}_{1:T}|\theta)]^{\phi_n} p(\theta)$, with $\phi_n \uparrow 1$, to add the information coming from the likelihood function in a gradual manner, without incurring sample degeneracy and impoverishment problems. Moreover, the SMC algorithm is “embarrassingly parallelizable” on multiple processors, thereby drastically reducing the computational time.

In our estimation we use a tempering schedule consisting of $N_\phi = 250$ bridge densities. The parameter λ , determining the convexity of the tempering schedule $\phi_n = \left(\frac{n-1}{N_\phi-1}\right)$, is set to 2.1, in order to retain substantial ESS in the first stages of the algorithm. The number of particles used is 80,000, entailing a total likelihood evaluation of 20 million. In line with Durham and Geweke (2014), we assess convergence by running the algorithm multiple times and comparing the estimates of parameters. The proposal, for the mutation step, is a random walk with an adaptive covariance matrix based on the information contained in the previous draws and with an adaptive scaling factor that targets an acceptance probability of 25%. Estimation is carried out on an AMD Ryzen 3900X processor with 24 threads and takes around 120 hours.

6.4 Estimation Results

The posterior means and standard deviations of parameters are shown in Table 3. The estimates suggest a high degree of habit formation. Posterior estimates indicate a higher

degree of stickiness in prices and wages in sector \mathcal{S}_1 with respect to that in sector \mathcal{S}_2 . The Taylor rule parameters do not move substantially from the values implied by the prior. Conversely, the likelihood proves to be influential in moving the autoregressive parameters from their diffuse priors, generally pointing to high degrees of persistence.

By running the filter using the parameters at the posterior means shown in Table 3, it

Table 3: Estimation Results. The table reports the parameter's name (Full Name) with the associated symbol (Symbol). The table also reports the prior shape (Prior), prior mean and standard deviation (Mean, St.Dev), and the posterior mean (Post. Mean) and standard deviation (Post. St.Dev) for the estimated parameters. The \mathcal{B} is the Beta distribution; \mathcal{N} is the Normal distribution; \mathcal{G} is the Gamma distribution; \mathcal{IG} is the Inverse-Gamma distribution; \mathcal{TN} is the Truncated Normal distribution on the interval (0, 1).

Full Name	Symbol	Prior	Mean,St.Dev.	Post. Mean	Post. St.Dev
Habits	h	\mathcal{B}	(0.70, 0.10)	0.81	0.02
Price rigidity \mathcal{S}_1	θ_1	\mathcal{B}	(0.50, 0.10)	0.71	0.02
Price rigidity \mathcal{S}_2	θ_2	\mathcal{B}	(0.50, 0.10)	0.69	0.02
Taylor rule inertia	r_R	\mathcal{B}	(0.75, 0.10)	0.57	0.03
Taylor rule output	r_Y	\mathcal{N}	(0.12, 0.05)	0.04	0.02
Taylor rule inflation	r_π	\mathcal{N}	(2.00, 0.15)	1.79	0.02
Persistence Prod. \mathcal{S}_1	ρ_{z_1}	\mathcal{B}	(0.50, 0.20)	0.98	0.01
Persistence Prod. \mathcal{S}_2	ρ_{z_2}	\mathcal{B}	(0.50, 0.20)	0.98	0.01
Persistence Intratemp.	ρ_j	\mathcal{B}	(0.50, 0.20)	0.99	0.00
Persistence Lab. Supply \mathcal{S}_1	ρ_{ϕ_1}	\mathcal{B}	(0.50, 0.20)	0.29	0.06
Persistence Intertemp.	ρ_ζ	\mathcal{B}	(0.50, 0.20)	0.40	0.08
Wage rigidity \mathcal{S}_1	θ_{w_1}	\mathcal{B}	(0.50, 0.10)	0.79	0.01
Wage rigidity \mathcal{S}_2	θ_{w_2}	\mathcal{B}	(0.50, 0.10)	0.54	0.03
Utiliz. adj.cost	η_u	\mathcal{B}	(0.50, 0.15)	0.93	0.03
Cap. adj.cost	η_k	\mathcal{G}	(10.00, 2.50)	7.94	0.60
St.Dev. Prod. \mathcal{S}_1	$100 \times \sigma_{z_1}$	\mathcal{IG}	(1.00, ∞)	0.69	0.05
St.Dev. Temp. Mon. Policy	$100 \times \sigma_e$	\mathcal{IG}	(1.00, ∞)	0.25	0.02
St.Dev. Prod. \mathcal{S}_2	$100 \times \sigma_{z_2}$	\mathcal{IG}	(1.00, ∞)	3.47	0.18
St.Dev. Intratemp.	$100 \times \sigma_j$	\mathcal{IG}	(1.00, ∞)	10.25	0.83
St.Dev. Pers. Mon. Policy	$100 \times \sigma_s$	\mathcal{IG}	(1.00, ∞)	3.25	0.30
St.Dev. Lab. Supply \mathcal{S}_1	$100 \times \sigma_{\phi_1}$	\mathcal{IG}	(1.00, ∞)	8.18	0.87
St.Dev. Lab. Supply \mathcal{S}_2	$100 \times \sigma_{\phi_2}$	\mathcal{IG}	(1.00, ∞)	2.77	0.42
St.Dev. Pref.	$100 \times \sigma_\zeta$	\mathcal{IG}	(1.00, ∞)	3.12	0.33
Prepandemic Dis. Prob.	$1000 \times \psi_{pre}$	\mathcal{TN}	(0.01, 0.10)	0.14	0.06
Postpandemic Dis. Prob.	$100 \times \psi_{post}$	\mathcal{TN}	(99.00, 1.00)	98.03	0.82

is possible to obtain the filtered estimates of shocks realization in the quarter 2020:Q2, which was severely impacted by the pandemic. With this parametrization, among all the possible combinations of large shocks as mentioned above, the filter detects the realization of a large shock to: (i) the labor supply in sector \mathcal{S}_1 ($\varepsilon_{\phi_1,t}$); (ii) the labor supply in sector \mathcal{S}_2 ($\varepsilon_{\phi_2,t}$); (iii) the utility of services consumption from sector \mathcal{S}_2 ($\varepsilon_{j,t}$); (iv) the demand in the consumption of both goods ($\varepsilon_{\zeta,t}$), (v) the labor productivity in sector \mathcal{S}_2 ($\varepsilon_{z_2,t}$); and (vi) the labor productivity in sector \mathcal{S}_1 ($\varepsilon_{z_1,t}$) (at the edge between being a

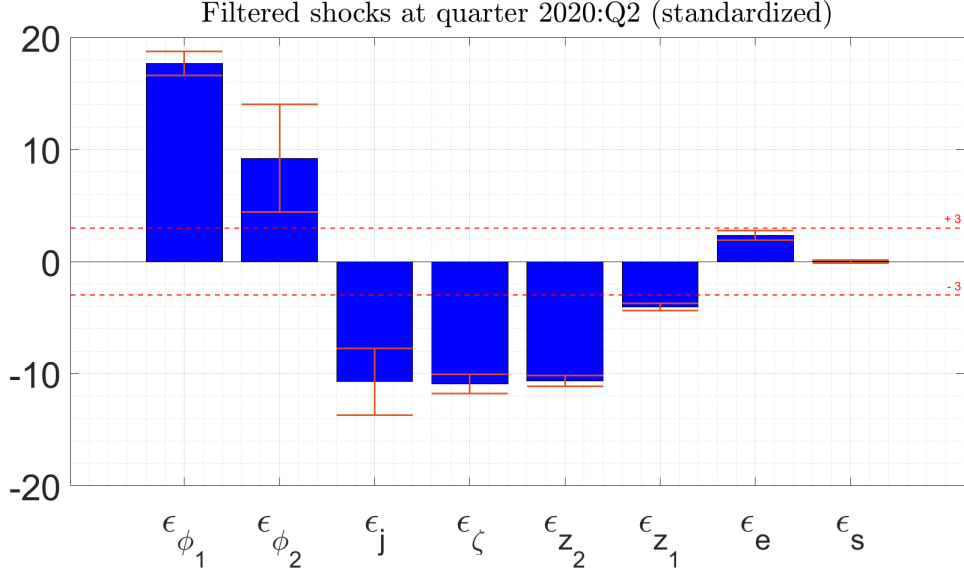


Figure 7: Filtered standardized shocks occurring in 2020:Q2. Bands represent one standard deviation resulting from parameter uncertainty. ϵ_{ϕ_1} : labor supply shock to \mathcal{S}_1 . ϵ_{ϕ_2} : labor supply shock to \mathcal{S}_2 . ϵ_j : demand shock to \mathcal{S}_2 services. ϵ_ζ : demand shocks to both sectors. ϵ_{z_2} : labor productivity shock to \mathcal{S}_2 . ϵ_{z_1} : labor productivity shock to \mathcal{S}_1 . ϵ_e : temporary monetary policy shock. ϵ_s : persistent monetary policy shock.

large and an ordinary shock, depending on parameter uncertainty). Figure 7 reports the filtered standardized shocks for 2020:Q2. The Figure shows that the filtered shocks for the first pandemic quarter display a magnified scale, resulting in innovations of one order of magnitude above the ordinary level. Overall, the scale of the filtered large shocks is in line with the monthly estimates of [Lenza and Primiceri \(2020\)](#) who find a factor of increase in variability of pandemic shocks in the range between one or two orders of magnitude with respect to the ordinary level. Figure 8 reports the results for 2020:Q3, showing the partial rebound of the US economy. The filter detects a combination of large shocks given by: (i) a large positive rebound shock to the intertemporal utility (ϵ_ζ); (ii) a rebound shock which drives down the disutility of working in sector \mathcal{S}_1 ($\epsilon_{\phi_1,t}$); (iii) a positive large shock to labor productivity in sector \mathcal{S}_1 ($\epsilon_{z_1,t}$); and (iv) a positive large shock to labor productivity in sector \mathcal{S}_2 ($\epsilon_{z_2,t}$). No clear large shock is detected, neither to the relative utility from \mathcal{S}_2 services nor to the labor supply to \mathcal{S}_2 .

The path of the autoregressive processes resulting from the large shocks as described above is displayed in Figure 9. Overall, the pandemic resulted in a large spike in the disutility of working in both sectors $\phi_{1,t}$ and $\phi_{2,t}$. While for sector \mathcal{S}_1 the labor disutility bounces back at Q3, it remains high for the pandemic-sensitive sector, \mathcal{S}_2 . As visible in the second row of Figure 9, labor productivity in the general sector $a_{z,1}$ returns back from the (relatively)

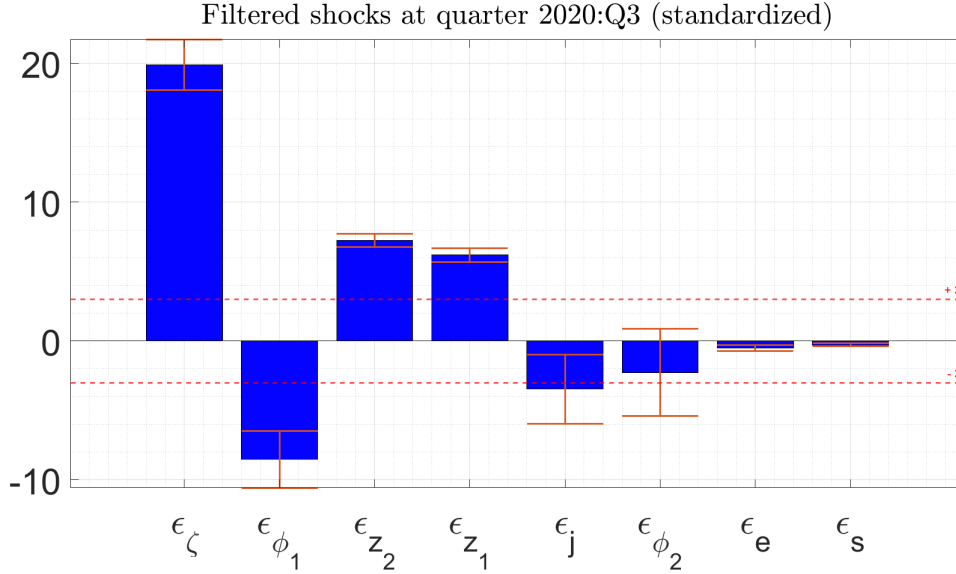


Figure 8: Filtered standardized shocks occurring in 2020:Q3. Bands represent one standard deviation resulting from parameter uncertainty. ε_ζ : demand shocks to both sectors. ε_{ϕ_1} : labor supply shock to \mathcal{S}_1 . ε_{z_2} : labor productivity shock to \mathcal{S}_2 . ε_{z_1} : labor productivity shock to \mathcal{S}_1 . ε_j : demand shock to \mathcal{S}_2 services. ε_{ϕ_2} : labor supply shock to \mathcal{S}_2 . ε_e : temporary monetary policy shock. ε_s : persistent monetary policy shock.

mild loss realized in Q2, while labor productivity in sector \mathcal{S}_2 does not fully recover from the massive fall of the first quarter. Concerning the intertemporal shock a_ζ , it bounces back far and beyond the prepandemic levels in Q3, while the intra-temporal utility shock a_j does not recover.

In a DSGE setting, it is not completely meaningful to classify a shock as a pure supply or demand shock, since each effect will be transmitted across the whole economy. It is always possible to stick to a practical definition that identifies a demand shock as one that drives quantities and prices in the same direction, and a supply shock as the opposite. This kind of definition leads to an immediate classification of the shocks in our DSGE model, providing a direct translation of the sign restrictions used in the SVAR context. From this perspective, the fact that supply shocks (e.g. labor supply and productivity) and demand shocks (e.g. intertemporal and intratemporal preference) are spotted together is in line with [Brinca et al. \(2020\)](#) who use a SVAR with sign restrictions.

To assess the impact of the identified large shocks on the observed series, a counterfactual analysis is provided. Given the nonlinearity of the system, a historical decomposition of the variables, in which the effects of individual shocks sum up perfectly to the observed series, cannot be constructed. We, therefore, evaluate the shocks relative importance by constructing an augmented state space, in which additional counterfactual variables

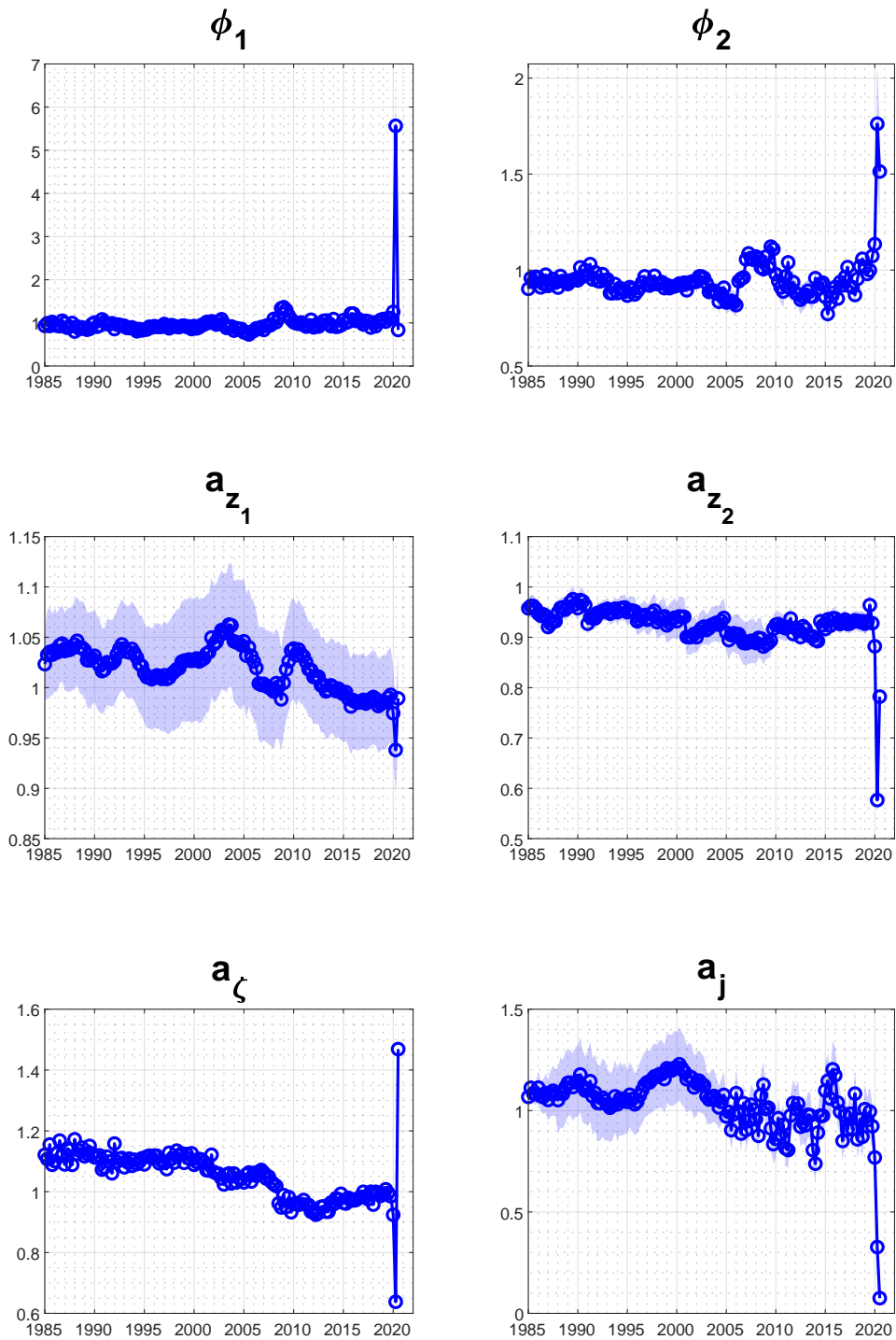


Figure 9: Filtered autoregressive processes. ϕ_1 : labor disutility in \mathcal{S}_1 . ϕ_2 : labor disutility in \mathcal{S}_2 . a_{z_1} : labor productivity in \mathcal{S}_1 . a_{z_2} : labor productivity in \mathcal{S}_2 . a_{ζ} : intertemporal preference. a_j : intratemporal preference.

are included. These variables track the scenarios in which some shocks are switched off, precisely:

$$\begin{aligned} \mathbf{y}_t &= A + B\mathbf{x}_t + u_t, & \mathbf{x}_t &= f(\mathbf{x}_{t-1} + R\tilde{\boldsymbol{\varepsilon}}_t), \\ \mathbf{y}_t^* &= A + B\mathbf{x}_t^* + u_t, & \mathbf{x}_t^* &= f(\mathbf{x}_{t-1} + R^*\tilde{\boldsymbol{\varepsilon}}_t). \end{aligned} \tag{61}$$

Equation (61) reports the augmented state space, for notational convenience model state and control variables are collapsed into the same vector $\mathbf{x}_t = [x_t^C \ x_t^S]'$ and the composite function $f(\cdot)$ combines $g(\cdot)$ and $h(\cdot)$. The matrix R^* is constructed by equating to zero the columns of R in correspondence of the shocks set to zero, to test what happens in the absence of them. This is done by looking at the filtered \mathbf{y}_t^* .

Figure 10 reports the counterfactual experiment for 2020:Q2. The bars represent the predicted response of the variables corresponding to the indicated shock, with the others set to zero. Interactions of shocks are non-negligible so that the sum of all individual contributions do not equate to the observed series.

As visible, the 8% drop in the production (ΔY_1) of sector \mathcal{S}_1 depends on different shocks pointing in the same direction, with the labor productivity being the most important. The 60%[†] drop in production (ΔY_2) in sector \mathcal{S}_2 is mostly due to the reduction in labor productivity (ε_{z_2}), which accounts for a reduction of 48%. The relative utility shock (ε_j) explains a drop in production by 16%. The decomposition of hours worked (second line of the plot) largely reflects the one in production.

Unlike the quantities, the decomposition of prices shows a more muted effect. Indeed, the limited response of prices compared to the large fall of quantities is a stark feature of the COVID-19 economic disruption, which suggests the coexistence of both supply and demand forces. As for inflation in sector \mathcal{S}_1 (π_1), the negative labor supply shock to that sector would have produced a 1.7% rate of inflation, as a counterfactual to the realized -1%. This is due to the negative intertemporal shock that drives down prices, and it would have produced a deflation of around -2% without the upward pressure caused by the reduction in labor supply. Concerning inflation in sector \mathcal{S}_2 (π_2) the bar plot shows that the negative labor supply shock (ε_{ϕ_2}) and the negative labor productivity shock (ε_{z_2}) outweigh

[†]The difference of logarithms becomes a crude approximation of the percentage drop in this case. Anyway, the log difference of data variables is connected to the log difference of model variables, so the poor approximation does not come with a wrong definition of the measurement equations.

the negative general demand (ε_ζ) and the sector-specific (ε_j) shocks. This produces the realized positive inflation of around 1%.

Turning to the wage inflation rates, similar counteracting dynamics between demand and supply shocks emerge. As for the wage inflation rate in sector \mathcal{S}_1 (ω_1), the large labor supply reduction, ε_{ϕ_1} , would have produced an increase in wages of around 6%, if the negative general demand shock had not brought it down to the realized 2%. Similarly, the labor supply reduction in sector \mathcal{S}_2 (ε_{ϕ_2}) would have driven the wage inflation, ω_2 to 4.6%, while the effect of the general demand shock (ε_ζ) summed to the sector specific one (ε_j) drives down the wage inflation in that sector to the realized level, -2%.

The drop in consumption is due to all the shocks moving in the same direction, with the general demand shock being the most important contributor. Notably, the general demand shock provides a positive contribution to investment, reducing the overall drop (the effects of the discount factor shock on consumption and investment in the same as in [Smets and Wouters, 2003](#)).

Finally, it is visible that supply shock, in the absence of demand shock, would have required a monetary tightening, as the price stability target by the central bank would have outweighed the output stabilization objective in that case.

In Figure 11, the shocks are grouped and aggregated into the supply and demand category. As in [Brinca et al. \(2020\)](#), the estimates of the relative effects of supply and demand shocks suggest a combination of the two. The estimates regarding sector \mathcal{S}_2 are broadly in line with the monthly results of [Brinca et al. \(2020\)](#).

7 Conclusion

This paper builds and estimates a two-sector medium-scale new Keynesian model to study the type, magnitude and direction of economic shocks during the pandemic. The model includes the standard real and nominal frictions used in the empirical literature and allows for heterogeneous COVID-19 pandemic exposure across sectors.

We solve the model nonlinearly and, to make inference, we propose a new nonlinear, Non-Gaussian filter (MM-CKF) designed to handle and identify the large pandemic shocks. Monte Carlo experiments show that our filter can correctly identify the source and time location of shocks and outperform Particle Filter based methods with a massively reduced

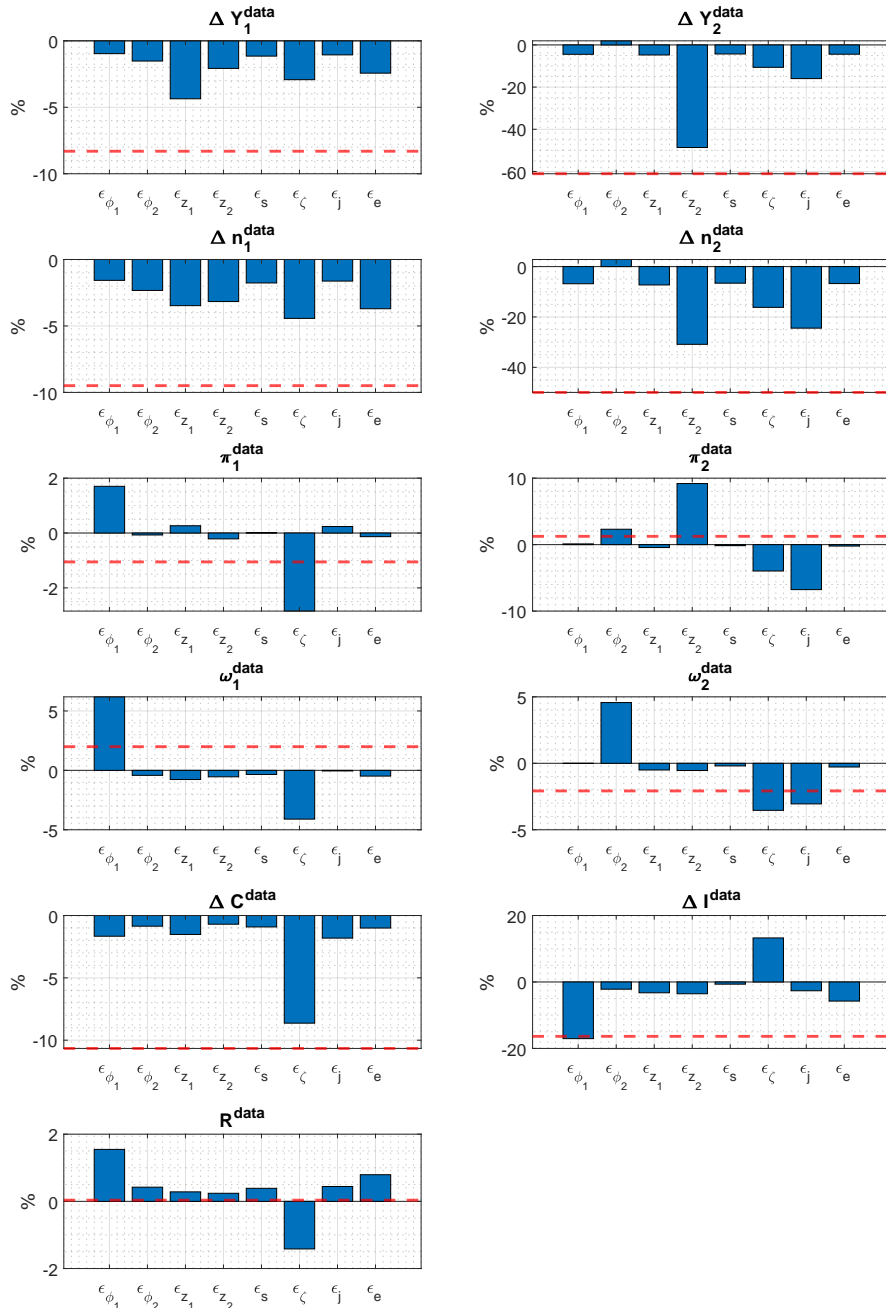


Figure 10: Contribution of individual shocks to the observed series for 2020:Q2. Each bar corresponds to the counterfactual in which only the reported shock is switched on. The red dotted line represents the realized values. Individual contributions do not add up to the observed series because of nonlinearity. The shocks are: demand shocks to both sectors (ϵ_{ζ}); labor supply shock to \mathcal{S}_1 (ϵ_{ϕ_1}); labor productivity shock to \mathcal{S}_2 (ϵ_{z_2}); labor productivity shock to \mathcal{S}_1 (ϵ_{z_1}); demand shock to \mathcal{S}_2 services (ϵ_j); labor supply shock to \mathcal{S}_2 (ϵ_{ϕ_2}); temporary monetary policy shock (ϵ_e) and the persistent monetary policy shock (ϵ_s).

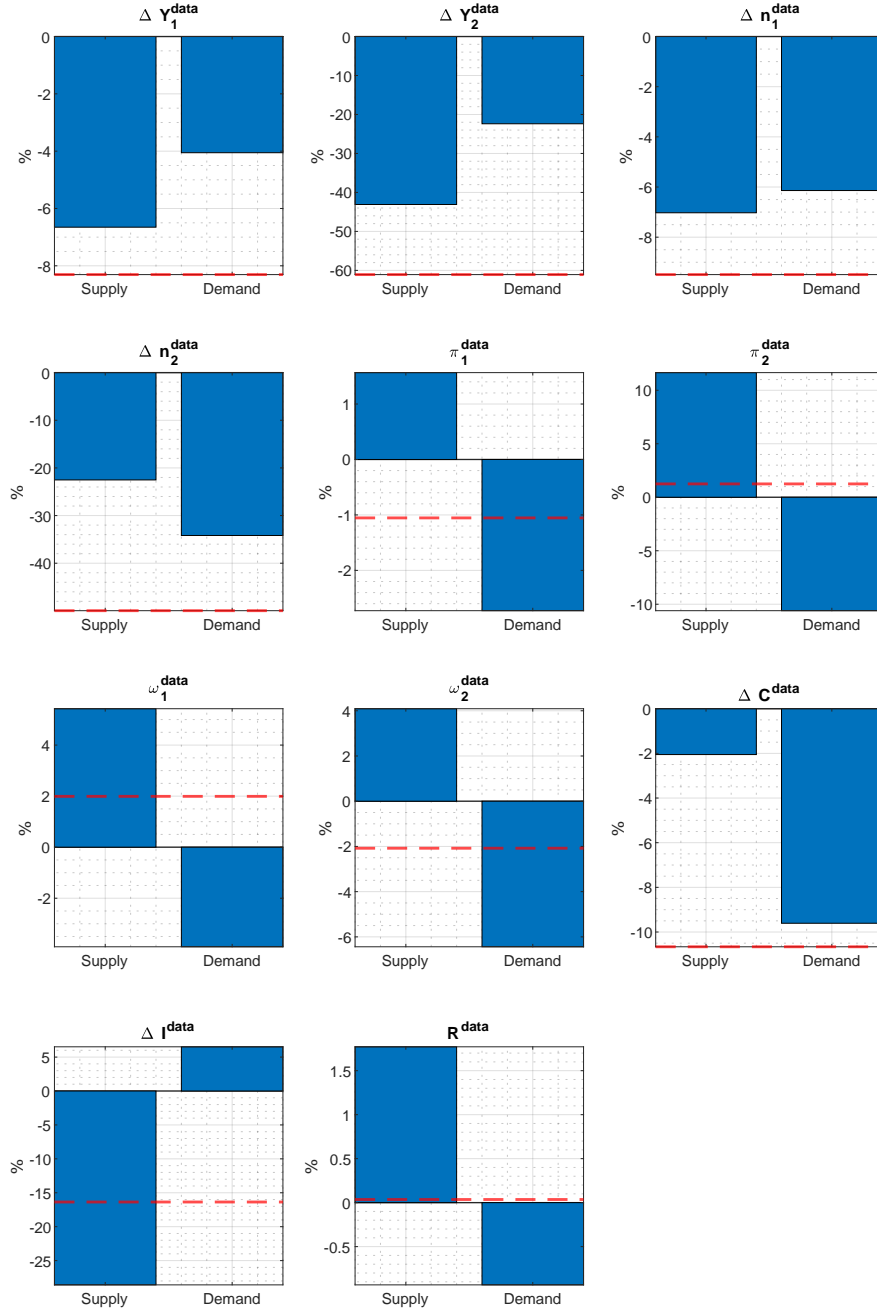


Figure 11: Contribution of groups of shocks to the observed series for 2020:Q2. The Demand (Supply) bars refer to the counterfactual with supply (demand) shocks switched down. Supply shocks: $\{\varepsilon_{\phi_1}, \varepsilon_{\phi_2}, \varepsilon_{z_1}, \varepsilon_{z_2}\}$. Demand shocks: $\{\varepsilon_j, \varepsilon_\zeta\}$. The red dotted line represents the realized values. Grouped contributions do not add up to the observed series because of nonlinearity.

running time. The reduced running time allows us to estimate the model using the Sequential Monte Carlo sampler recently proposed by [Herbst and Schorfheide \(2014\)](#).

The main empirical result of the paper is to show that the economic disruption caused by the COVID-19 pandemic is not attributable to the realization of shocks of the supply or

demand kind alone, but rather to a combination of those.

Treating the pandemic shocks as exogenous is undoubtedly a limitation of this exercise with respect to the microfoundation paradigm. Nonetheless, it can still be considered as a first step before putting a fully-fledged DSGE model with an integrated epidemiological block to the data, which could in turn help to take a normative view about the optimal combination of health and economic policies.

The availability of new data points related to the evolution of the pandemic will enable the continuation of the analysis. New data will also allow testing for parameters stability with respect to the ongoing pandemic shocks. Also, and importantly, as time goes by, it will become possible to distinguish how much of the COVID-19 episode resulted in large shocks to the cycle and how much to the trend. Indeed, to allow for large shocks to non-stationary productivity variables inside the model or to reduced-form trend components in the measurement equations, would require simple modifications to the methodology applied in this contribution.

References

- Abo-Zaid, S. and Xuguang, S. S. (2020). Health Shocks in a General Equilibrium Model. *Available at SSRN: <https://ssrn.com/abstract=3611404>.*
- Alspach, D. and Sorenson, H. (1972). Nonlinear Bayesian Estimation Using Gaussian Sum Approximations. *IEEE transactions on automatic control*, 17:439–448.
- Amisano, G. and Tristani, O. (2010). Euro Area Inflation Persistence in an Estimated Nonlinear DSGE model. *Journal of Economic Dynamics and Control*, 34:1837–1858.
- Amisano, G. and Tristani, O. (2011). Exact Likelihood Computation for Nonlinear DSGE Models with Heteroskedastic Innovations. *Journal of Economic Dynamics and Control*, 35:2167–2185.
- An, S. and Schorfheide, F. (2007). Bayesian Analysis of DSGE Models. *Econometric reviews*, 26:113–172.
- Andreasen, M. M. (2011). Non-Linear DSGE Models and the Optimized Central Difference Particle Filter. *Journal of Economic Dynamics and Control*, 35:1671–1695.

- Andreasen, M. M. (2012). An Estimated DSGE Model: Explaining Variation in Nominal Term Premia, Real Term Premia, and Inflation Risk Premia. *European Economic Review*, 56:1656–1674.
- Andreasen, M. M. (2013). Non-linear DSGE Models and the Central Difference Kalman Filter. *Journal of Applied Econometrics*, 28:929–955.
- Arasaratnam, I. and Haykin, S. (2009). Cubature Kalman Filters. *IEEE Transactions on automatic control*, 54:1254–1269.
- Arasaratnam, I., Haykin, S., and Elliott, R. J. (2007). Discrete-time Nonlinear Filtering Algorithms using Gauss–Hermite Quadrature. *Proceedings of the IEEE*, 95:953–977.
- Aruoba, S. B., Cuba-Borda, P., Higa-Flores, K., Schorfheide, F., and Villalvazo, S. (2021). Piecewise-Linear Approximations and Filtering for DSGE Models with Occasionally Binding Constraints. *Review of Economic Dynamics*, *Forthcoming*.
- Baqae, D. R. and Farhi, E. (2021). Supply and Demand in Disaggregated Keynesian Economies with an Application to the Covid-19 Crisis. NBER Working Paper N. 27152.
- Bengtsson, T., Bickel, P., Li, B., et al. (2008). Curse-of-Dimensionality Revisited: Collapse of the Particle Filter in Very Large Scale Systems. In *Probability and statistics: Essays in honor of David A. Freedman*, pages 316–334. Institute of Mathematical Statistics.
- Benigno, G., Foerster, A., Otrok, C., and Rebucci, A. (2020). Estimating Macroeconomic Models of Financial Crises: An Endogenous Regime-Switching Approach. NBER Working Paper N. 26935.
- Bernanke, B. S., Gertler, M., and Gilchrist, S. (1999). The Financial Accelerator in a Quantitative Business Cycle Framework. *Handbook of macroeconomics*, 1:1341–1393.
- Binning, A. and Maih, J. (2015). Sigma Point Filters for Dynamic Nonlinear Regime Switching Models. Norges Bank Working Paper N. 10—2015.
- Bodenstein, M., Corsetti, G., and Guerrieri, L. (2020). Social Distancing and Supply Disruptions in a Pandemic. CEPR Discussion Paper N. DP14629.

- Brinca, P., Duarte, J. B., and Faria-e Castro, M. (2020). Measuring Sectoral Supply and Demand Shocks During COVID-19. Federal Reserve Board St.Louis Working paper 2020-011.
- Cai, M., Del Negro, M., Herbst, E., Matlin, E., Sarfati, R., and Schorfheide, F. (2021). Online Estimation of DSGE Models. *The Econometrics Journal*, 24:33–58.
- Christiano, L. J., Eichenbaum, M., and Evans, C. L. (2005). Nominal Rigidities and the Dynamic Effects of a Shock to Monetary Policy. *Journal of Political Economy*, 113:1–45.
- Creal, D. (2007). Sequential Monte Carlo Samplers for Bayesian DSGE Models. *Manuscript, University Chicago Booth*, pages 245–296.
- Del Negro, M. and Schorfheide, F. (2008). Forming Priors for DSGE Models (and How it Affects the Assessment of Nominal Rigidities). *Journal of Monetary Economics*, 55:1191–1208.
- del Rio-Chanona, R. M., Mealy, P., Pichler, A., Lafond, F., and Farmer, J. D. (2020). Supply and Demand Shocks in the COVID-19 Pandemic: An Industry and Occupation Perspective. *Oxford Review of Economic Policy*, 36:94–137.
- Dewachter, H. and Wouters, R. (2014). Endogenous Risk in a DSGE Model with Capital-Constrained Financial Intermediaries. *Journal of Economic Dynamics and control*, 43:241–268.
- Durham, G. and Geweke, J. (2014). Adaptive Sequential Posterior Simulators for Massively Parallel Computing Environments. In *Bayesian model comparison*. Emerald Group Publishing Limited.
- Eichenbaum, M. S., Rebelo, S., and Trabandt, M. (2020a). Epidemics in the Neoclassical and New Keynesian Models. NBER Working Paper N. 27430.
- Eichenbaum, M. S., Rebelo, S., and Trabandt, M. (2020b). The Macroeconomics of Epidemics. NBER Working Paper N. 26882.
- Faria-e Castro, M. (2021). Fiscal Policy During a Pandemic. *Journal of Economic Dynamics & Control*, (Forthcoming).

- Faubel, F., McDonough, J., and Klakow, D. (2009). The Split and Merge Unscented Gaussian Mixture Filter. *IEEE Signal Processing Letters*, 16:786–789.
- Fernández-Villaverde, J., Guerrón-Quintana, P., Rubio-Ramírez, J. F., and Uribe, M. (2011). Risk Matters: The Real Effects of Volatility Shocks. *American Economic Review*, 101:2530–61.
- Fernández-Villaverde, J. and Rubio-Ramírez, J. F. (2007). Estimating Macroeconomic Models: A Likelihood Approach. *The Review of Economic Studies*, 74:1059–1087.
- Flury, T. and Shephard, N. (2011). Bayesian Inference Based Only on Simulated Likelihood: Particle Filter Analysis of Dynamic Economic Models. *Econometric Theory*, 27:933–956.
- Fornaro, L. and Wolf, M. (2020a). Covid-19 Coronavirus and Macroeconomic Policy. CEPR Discussion Paper N. DP14529.
- Fornaro, L. and Wolf, M. (2020b). The Scars of Supply Shocks. CEPR Discussion Paper N. DP15423.
- Gordon, N. J., Salmond, D. J., and Smith, A. F. (1993). Novel Approach to Nonlinear/Non-Gaussian Bayesian State Estimation. In *IEE proceedings F (radar and signal processing)*, volume 140, pages 107–113.
- Guerrieri, V., Lorenzoni, G., Straub, L., and Werning, I. (2020). Macroeconomic Implications of COVID-19: Can Negative Supply Shocks Cause Demand Shortages? NBER Working Paper N. 26918.
- Herbst, E. and Schorfheide, F. (2014). Sequential Monte Carlo Sampling for DSGE Models. *Journal of Applied Econometrics*, 29:1073–1098.
- Herbst, E. P. and Schorfheide, F. (2015). *Bayesian Estimation of DSGE Models*. Princeton University Press.
- Iacoviello, M. and Neri, S. (2010). Housing Market Spillovers: Evidence from an Estimated DSGE Model. *American Economic Journal: Macroeconomics*, 2:125–64.
- Ito, K. and Xiong, K. (2000). Gaussian Filters for Nonlinear Filtering Problems. *IEEE transactions on automatic control*, 45:910–927.

- Ivashchenko, S. (2014). DSGE Model Estimation on the Basis of Second-Order Approximation. *Computational Economics*, 43:71–82.
- Jia, B., Xin, M., and Cheng, Y. (2013). High-Degree Cubature Kalman Filter. *Automatica*, 49:510–518.
- Kaplan, G., Moll, B., and Violante, G. L. (2020). The Great Lockdown and the Big Stimulus: Tracing the Pandemic Possibility Frontier for the US. NBER Working Paper N. 27794.
- Kollmann, R. (2015). Tractable Latent State Filtering for Non-linear DSGE Models Using a Second-Order Approximation and Pruning. *Computational Economics*, 45:239–260.
- Kotecha, J. H. and Djuric, P. M. (2003). Gaussian-Sum Particle Filtering. *IEEE Transactions on signal processing*, 51:2602–2612.
- Lenza, M. and Primiceri, G. E. (2020). How to Estimate a VAR after March 2020. Technical report, National Bureau of Economic Research.
- Leong, P. H., Arulampalam, S., Lamaheewa, T. A., and Abhayapala, T. D. (2013). A Gaussian-Sum Based Cubature Kalman Filter for Bearings-Only Tracking. *IEEE Transactions on Aerospace and Electronic Systems*, 49:1161–1176.
- Levintal, O. (2017). Fifth-Order Perturbation Solution to DSGE Models. *Journal of Economic Dynamics and Control*, 80:1–16.
- Liu, J. S. and Chen, R. (1998). Sequential Monte Carlo Methods for Dynamic Systems. *Journal of the American Statistical Association*, 93:1032–1044.
- Noh, S. (2019). Posterior Inference on Parameters in a Nonlinear DSGE Model via Gaussian-Based Filters. *Computational Economics*, pages 1–47.
- Pei, H. L., Arulampalam, S., Lamaheewa, A. T., and Abhayapala, D. T. (2013). A Gaussian-Sum Based Cubature Kalman Filter for Bearings-Only Tracking. *IEEE Transactions on Aerospace and Electronic Systems*, 49:1161–1176.
- Pei, H. L., Arulampalam, S., Lamaheewa, A. T., and Abhayapala, D. T. (2014). Gaussian-Sum Cubature Kalman Filter with Improved Robustness for Bearings-only Tracking. *IEEE Signal Processing Letters*, 21:513–517.

- Pitt, M. K. and Shephard, N. (1999). Filtering Via Simulation: Auxiliary Particle Filters. *Journal of the American Statistical Association*, 94:590–599.
- Särkkä, S. (2013). *Bayesian Filtering and Smoothing*. Cambridge University Press.
- Smets, F. and Wouters, R. (2003). An Estimated Dynamic Stochastic General Equilibrium Model of the Euro Area. *Journal of the European Economic Association*, 1:1123–1175.
- Smets, F. and Wouters, R. (2007). Shocks and Frictions in US Business Cycles: A Bayesian DSGE Approach. *American Economic Review*, 97:586–606.
- Sorenson, H. W. and Alspach, D. L. (1971). Recursive Bayesian Estimation using Gaussian-Sums. *Automatica*, 7:465–479.
- Wan, E. A. and Van Der Merwe, R. (2000). The Unscented Kalman Filter for Nonlinear Estimation. *Proceedings of the IEEE 2000 Adaptive Systems for Signal Processing, Communications, and Control Symposium*, 1:153–158.
- Woodford, M. (2020). Effective Demand Failures and the Limits of Monetary Stabilization Policy. NBER Working Paper N. 27768.

Appendix A: Data Construction

Gross domestic product

Real gross domestic product (GDP) is retrieved from the U.S. Bureau of Economic Analysis series GDPC1. The series is seasonally adjusted and is expressed as billions of chained 2012 dollars. The GDP is divided by the Civilian Noninstitutional Population (series CNP16OV from the U.S. Bureau of Labor Statistics) to transform it in per capita terms. Sectoral data is obtained from the GDP-by-industry accounts from the U.S. Bureau of Economic Analysis. The shares of GDP as a percentage of total added value are reported for the following classification of the U.S. industries, from which the GDP series for the two sectors of the model are obtained:

- Agriculture, forestry, fishing, and hunting; Mining; Utilities; Construction; Manufacturing; Wholesale trade; Retail trade; Transportation and warehousing; Information; Finance, insurance, real estate, rental, and leasing; Professional and business services; Educational services, health care, and social assistance; Other services, except government; Federal government; State and local government.
- Arts, entertainment, recreation, accommodation, and food services.

Data is available annually until 2005:Q1 and at quarterly frequencies afterwards. The missing quarters are handled as missing data by the MM-CKF, setting to zero the corresponding Kalman gain entries. The data spans from 1985:Q1 to 2020:Q3.

Inflation

Sectoral data on prices are collected by the U.S. Bureau of Economic Analysis in the GDP-by-industry accounts. For each sector, chain-type price indexes are collected, with 2012 being the reference year. As for value-added by sectors, quarterly data is only available starting from 2005:Q1. Only one out of four quarterly inflation rates are therefore assumed to be observed for each year before 2005 and it is assumed to be equal to the yearly rate divided by four. The other observations are treated as missing. The data spans from 1985:Q1 to 2020:Q3.

Consumption

Aggregate real consumption in billions of chained 2012 dollars is provided by the U.S. Bureau of Economic Analysis in the PCECC96 series. The series is seasonally adjusted and it spans from 1985:Q1 to 2020:Q3. The series is divided by the Population Level (CNP16OV) to get per capita consumption.

Investment

Real Gross Private Domestic Investment is retrieved from the U.S. Bureau of Economic Analysis series GPDIC1. It is seasonally adjusted and measured in billions of chained 2012 dollars and it spans from 1985:Q1 to 2020:Q3. The series is divided by the Population Level (CNP16OV) to get per capita investment.

Hours worked

Data on hours worked across industries is obtained from the U.S. Bureau of Labor Statistics's Current Employment Statistics (Establishment Survey). In Table B-7, the average weekly hours and overtime of production and nonsupervisory employees on private non-farm payrolls is collected, while the number of employees on nonfarm payrolls for each industry is found in Table B-1. The original monthly series are filtered to the quarterly frequency by applying the arithmetic mean. All series are seasonally adjusted. The per capita weekly hours worked in each sector are obtained by multiplying the average hours by employment and dividing them by the Population Level (CNP16OV). The data spans from 1985:Q1 to 2020:Q3.

Wages

Data on sectoral nominal wages is retrieved from the Current Employment Statistics (Establishment Survey) provided by U.S. Bureau of Labor Statistics. Average hourly earnings of production and nonsupervisory employees for the various industries are found in Table B-8. Monthly seasonally adjusted data is averaged to obtain quarterly figures. Nominal wages for aggregate subsets of sectors is obtained as a weighted average of wages with respect to hours worked in that sectors. We differentiate logged data to get nominal wage inflation. The data spans from 1985:Q1 to 2020:Q3.

Interest rate

The nominal short-term interest rate is measured as the 3-Month Treasury Bill yield in the secondary market. The daily measurements are averaged and divided by four to get the quarterly interest rate. The data spans from 1985:Q1 to 2020:Q3.

Appendix B: Steady State

Here we derive the steady state of the model.

$$\begin{aligned} X_1 &= \frac{\epsilon_{\pi_1}}{\epsilon_{\pi_1} - 1}, & X_2 &= \frac{\epsilon_{\pi_2}}{\epsilon_{\pi_2} - 1}, & X_{w_1} &= \frac{\epsilon_{w_1}}{\epsilon_{w_1} - 1}, \\ X_{w_2} &= \frac{\epsilon_{w_2}}{\epsilon_{w_2} - 1}, & uk_1 &= 1, & uk_2 &= 1, & \pi_1 &= 1, \\ \pi_2 &= 1, & \Psi_{k_1} &= 0, & \Psi_{k_2} &= 0, & \Psi_{u_1} &= 0, & \Psi_{u_2} &= 0. \end{aligned}$$

The parameter R_{ss} , appearing in the Taylor rule and pinning down the steady state for the unconstrained interest rate R_{unc} , is calibrated to be the root of the barrier polynomial $R = c_0 + c_1 R_{unc} + c_2 R_{unc}^2$ (the economically admissible one of the two), so that:

$$R_{unc} = R_{ss}$$

and

$$R = \frac{1}{\beta}.$$

The auxiliary variables ζ_0 , ζ_1 , ζ_2 and ζ_3 are defined for the sake of convenience. The variables ζ_0 and ζ_1 are respectively equal to $\frac{k_1}{Y_1}$ and $\frac{k_2}{Y_2}$, while ζ_2 and ζ_3 stand for $\frac{c_1}{Y_1}$ and $\frac{c_2}{Y_2}$, respectively. It holds that:

$$\begin{aligned} \zeta_0 &= \frac{\alpha_1 \beta}{X_1(1 - \beta(1 - \delta_{k_1}))}, & \zeta_1 &= \frac{\alpha_2 \beta}{X_2(1 - \beta(1 - \delta_{k_2}))}, & \zeta_3 &= 1, \\ n_2 &= \left(\frac{1 - \alpha_2}{X_2 X_{w_2}} \frac{1}{\zeta_3} \frac{j^{ss}}{\phi_2^{ss}} \right)^{\frac{1}{1+\nu_2}}, & Y_2 &= n_2 \zeta_1^{\frac{\alpha_2}{1-\alpha_2}}, & k_2 &= \zeta_1 Y_2, & c_2 &= \zeta_3 Y_2. \end{aligned}$$

The ratio between c_1 and p_2 can be easily found as:

$$c_1/p_2 = \frac{c_2}{j^{ss}}.$$

Then, by the market clearing for Sector 1,

$$Y_1/p_2 = \frac{c_1/p_2 + \delta_{k_2}k_2}{1 - \delta_{k_1}\zeta_0},$$

so that

$$\zeta_2 = \frac{c_1/p_2}{Y_1/p_2}, \quad n_1 = \left(\frac{1 - \alpha_1}{X_1 X_{w_1}} \frac{1}{\zeta_2} \frac{1}{\phi_1^{ss}} \right)^{\frac{1}{1+\nu_1}}, \quad Y_1 = n_1 \zeta_0^{\frac{\alpha_1}{1-\alpha_1}}, \quad k_1 = \zeta_0 Y_1,$$

$$c_1 = \zeta_2 Y_1, \quad uc_1 = \frac{1}{c_1}, \quad uc_2 = \frac{j^{ss}}{c_2}, \quad w_1 = \phi_1^{ss} n_1^{\nu_1} \frac{X_{w_1}}{uc_1},$$

$$w_2 = \phi_2^{ss} n_2^{\nu_2} \frac{X_{w_2}}{uc_2}, \quad p_2 = \frac{uc_2}{uc_1}, \quad \Pi_{r_1} = \left(1 - \frac{1}{X_1} \right) Y_1, \quad \Pi_{r_2} = \left(1 - \frac{1}{X_2} \right) Y_2,$$

$$\Pi_{u_1} = \left(1 - \frac{1}{X_{w_1}} \right) w_1 n_1, \quad \Pi_{u_2} = \left(1 - \frac{1}{X_{w_2}} \right) w_2 n_2, \quad \pi = \pi_1 \left(\frac{Y_1}{Y_1 + p_2 Y_2} \right) \pi_2 \left(\frac{p_2 Y_2}{Y_1 + p_2 Y_2} \right) = 1,$$

$$a_{z_1} = 1, \quad a_{z_2} = 1, \quad a_j = j^{ss}, \quad a_s = 1, \quad \phi_1 = \phi_1^{ss}, \quad \phi_2 = \phi_2^{ss}.$$

Appendix C: Derivation of the Mixture of Mixture Cubature

Kalman Filter

This Appendix describes in detail the derivation of the Mixture of Mixture of Cubature Kalman Filter (MM-CKF). The MM-CKF is based on the Cubature Kalman Filter (CKF) of [Arasaratnam and Haykin \(2009\)](#). The CKF falls into the category of Gauss-Hermite transformation filters, where the moments' propagation and updating are based on numerical integration rules. Differently from the Gauss-Hermite Kalman filter (GHKF) of [Ito](#)

and Xiong (2000) and the Quadrature Kalman filter (QKF) of Arasaratnam et al. (2007), the number of sigma points scales linearly in the integration dimensions, by the use of symmetric spherical-radial cubature rule. This provides a tool against the curse of dimensionality. The spherical radial cubature rule in Arasaratnam and Haykin (2009) is exact up to order three, meaning that the first moments will be propagated exactly for state-space functions consisting in polynomials up to order three (or well approximated by polynomials up to order three). As pointed out by Särkkä (2013), indeed, the integrations involving second moments will be exact just for state-space functions consisting of polynomials up to order one. It is possible to specify high order Cubature Kalman filters (Jia et al., 2013), but the number of cubature points would scale polynomially in the state dimension. Moreover, some weights may turn negative, possibly giving rise to numerical instability. The algorithm of the CKF is the following: Assuming $p(x_0^S | \mathbf{y}_{1:0}) = \mathcal{N}(m_{0|0}, P_{0|0})$ the initial distribution of the states, for $t = 1$ to T perform the following steps:

1) Prediction

- (a) From time $t-1$ posterior density function $p(x_{t-1}^S | \mathbf{y}_{1:t-1}) = \mathcal{N}(m_{t-1|t-1}, P_{t-1|t-1})$ form the augmented filtered cubature points:

$$\begin{pmatrix} \mathcal{X}_{t-1|t-1}^{S(i)} \\ \boldsymbol{\xi}_{t-1|t-1}^{(i)} \end{pmatrix} = \begin{pmatrix} m_{t-1|t-1} \\ \mathbb{E}(\boldsymbol{\varepsilon}_t) \end{pmatrix} + \sqrt{\begin{pmatrix} P_{t-1|t-1} & 0 \\ 0 & \mathbb{V}(\boldsymbol{\varepsilon}_t) \end{pmatrix}} \boldsymbol{\xi}^{(i)}$$

$$i = 1, \dots, 2(n_x^S + n_\varepsilon)$$

where the cubature points $(\boldsymbol{\xi}^{(i)})$ are derived from the spherical-radial rule (Arasaratnam and Haykin, 2009)

$$\boldsymbol{\xi}^{(i)} = \begin{cases} \sqrt{n_x^S + n_\varepsilon} \mathbf{e}_i, & i = 1, \dots, n_x^S + n_\varepsilon, \\ -\sqrt{n_x^S + n_\varepsilon} \mathbf{e}_{i-n_x^S-n_\varepsilon}, & i = n_x^S + n_\varepsilon + 1, \dots, 2(n_x^S + n_\varepsilon), \end{cases}$$

and where the \mathbf{e}_i 's are the vectors forming the standard basis of $\mathbb{R}^{(n_x^S + n_\varepsilon)}$.

- (b) Propagate states cubature points using the second equation in (54):

$$\mathcal{X}_{t|t-1}^{S(i)} = h(\mathcal{X}_{t-1|t-1}^{S(i)}) + R\boldsymbol{\varepsilon}_{t-1|t-1}^{(i)}, \quad i = 1, \dots, 2(n_x^S + n_\varepsilon)$$

(c) Obtain predicted controls cubature points using the first equation in (54):

$$\mathcal{X}_{t|t-1}^{C^{(i)}} = g \left(\mathcal{X}_{t|t-1}^{S^{(i)}} \right), \quad i = 1, \dots, 2(n_x^S + n_\varepsilon)$$

(d) Compute predicted means and covariances for states and controls

$$\mu_{t|t-1}^* \equiv \begin{pmatrix} m_{t|t-1}^S \\ m_{t|t-1}^C \end{pmatrix} = \frac{1}{2(n_x^S + n_\varepsilon)} \sum_{i=1}^{2(n_x^S + n_\varepsilon)} \begin{pmatrix} \mathcal{X}_{t|t-1}^{S^{(i)}} \\ \mathcal{X}_{t|t-1}^{C^{(i)}} \end{pmatrix}$$

$$P_{t|t-1}^* = \frac{1}{2(n_x^S + n_\varepsilon)} \sum_{i=1}^{2(n_x^S + n_\varepsilon)} \left\{ \left[\begin{pmatrix} \mathcal{X}_{t|t-1}^{S^{(i)}} \\ \mathcal{X}_{t|t-1}^{C^{(i)}} \end{pmatrix} - \begin{pmatrix} m_{t|t-1}^S \\ m_{t|t-1}^C \end{pmatrix} \right] \left[\begin{pmatrix} \mathcal{X}_{t|t-1}^{S^{(i)}} \\ \mathcal{X}_{t|t-1}^{C^{(i)}} \end{pmatrix} - \begin{pmatrix} m_{t|t-1}^S \\ m_{t|t-1}^C \end{pmatrix} \right]' \right\}'$$

2) Updating

(a) Form the predicted states and controls cubature points:

$$\mathcal{X}_{t|t-1}^{*(i)} = \mu_{t|t-1}^* + \sqrt{P_{t|t-1}^*} \zeta^{(i)}, \quad i = 1, \dots, 2(n_x^S + n_x^C)$$

(b) Obtain predicted observations cubature points through the measurement equation (55):

$$\mathcal{Y}_{t|t-1}^{(i)} = A + B\mathcal{X}_{t|t-1}^{*(i)}, \quad i = 1, \dots, 2(n_x^S + n_x^C).$$

(c) Compute predicted observables mean, covariance and cross-covariance between the states and observables:

$$\bar{\mathcal{Y}}_{t|t-1} = \frac{1}{2(n_x^S + n_x^C)} \sum_{i=1}^{2(n_x^S + n_x^C)} \mathcal{Y}_{t|t-1}^{(i)}$$

$$\mathcal{F}_{t|t-1} = \frac{1}{2(n_x^S + n_x^C)} \sum_{i=1}^{2(n_x^S + n_x^C)} \left(\mathcal{Y}_{t|t-1}^{(i)} - \bar{\mathcal{Y}}_{t|t-1} \right) \left(\mathcal{Y}_{t|t-1}^{(i)} - \bar{\mathcal{Y}}_{t|t-1} \right)' + \mathbb{V}(u_t)$$

$$\mathcal{P}_{t|t-1}^{xy} = \frac{1}{2(n_x^S + n_x^C)} \sum_{i=1}^{2(n_x^S + n_x^C)} \left(\mathcal{X}_{t|t-1}^{*(i)} - \mu_{t|t-1}^* \right) \left(\mathcal{Y}_{t|t-1}^{(i)} - \bar{\mathcal{Y}}_{t|t-1} \right)'$$

- (d) Compute Kalman gain to obtain the new filtered mean and covariance for states and controls:

$$\begin{aligned}\mathcal{K}_t &= \mathcal{P}_{t|t-1}^{xy} (\mathcal{F}_{t|t-1})^{-1} \\ \mu_{t|t}^* &= \mu_{t|t-1}^* + \mathcal{K}_t (y_t - \bar{\mathcal{Y}}_{t|t-1}) \\ P_{t|t}^* &= P_{t|t-1}^* - \mathcal{P}_{t|t-1}^{xy} (\mathcal{F}_{t|t-1})^{-1} \left(\mathcal{P}_{t|t-1}^{xy} \right)'\end{aligned}$$

From $\mu_{t|t}^*$ and $P_{t|t}^*$ the n_x^S states entries are retained to have $m_{t|t}$ and $P_{t|t}$ to be used in the following iteration.

The MM-CKF described in Section 5 is based on a mixture of mixture of CKF. This mixture is on the structural errors allowing to disentangle the structural shock that experience the large negative (positive) impulse. The MM-CKF is the following:

Assume $p(x_0^S | \mathbf{y}_{1:0}) = \mathcal{N}(m_{0|0}, P_{0|0})$ as the initial distribution of the states, and $G_0 = 1$. For $t = 1, \dots, T$ and for each filtered component $n = 1, \dots, G_{t-1}$ in

$$p(\mathbf{x}_{t-1} | \mathbf{y}_{1:t-1}) = \sum_{n=1}^{G_{t-1}} p(\mathbf{x}_{t-1} | \kappa_{t-1}^n, \mathbf{y}_{1:t-1}) p(\kappa_t^n | \mathbf{y}_{1:t}) = \sum_{n=1}^{G_{t-1}} \mathcal{N}(m_{t-1|t-1}^n, P_{t-1|t-1}^n) w_{t-1|t-1}^n.$$

perform the following steps:

1) Prediction

- (a) Split each filter n in K densities with predicted weights $\tilde{w}_{t|t-1}^{n,k} = w_{t-1|t-1}^n \psi_k$, $k = 1, \dots, K$, assuming noise from component $\boldsymbol{\varepsilon}_t^k$.
- (b) For each shock component $k = 1, \dots, K$ form the augmented filtered cubature points:

$$\begin{aligned}\begin{pmatrix} \mathcal{X}_{t-1|t-1}^{n,k,S^{(i)}} \\ \boldsymbol{\varepsilon}_{t-1|t-1}^{n,k,(i)} \end{pmatrix} &= \begin{pmatrix} m_{t-1|t-1}^n \\ \mathbb{E}(\boldsymbol{\varepsilon}_t^k) \end{pmatrix} + \sqrt{\begin{pmatrix} P_{t-1|t-1}^n & 0 \\ 0 & \mathbb{V}(\boldsymbol{\varepsilon}_t^k) \end{pmatrix}} \boldsymbol{\xi}^{(i)} \\ & i = 1, \dots, 2(n_x^S + n_\varepsilon).\end{aligned}$$

- (c) Propagate states cubature points using equation (54):

$$\mathcal{X}_{t|t-1}^{n,k,S^{(i)}} = h \left(\mathcal{X}_{t-1|t-1}^{n,k,S^{(i)}} \right) + R \boldsymbol{\varepsilon}_{t-1|t-1}^{n,k,(i)}, \quad i = 1, \dots, 2(n_x^S + n_\varepsilon).$$

(d) Obtain predicted controls cubature points using equation (54):

$$\mathcal{X}_{t|t-1}^{n,k,C^{(i)}} = g \left(\mathcal{X}_{t|t-1}^{n,k,S^{(i)}} \right), \quad i = 1, \dots, 2(n_x^S + n_\varepsilon).$$

(e) Compute predicted means and covariances for states and controls:

$$\begin{aligned} \mu_{t|t-1}^{*,n,k} &\equiv \begin{pmatrix} m_{t|t-1}^{n,k,S} \\ m_{t|t-1}^{n,k,C} \end{pmatrix} = \frac{1}{2(n_x^S + n_\varepsilon)} \sum_{i=1}^{2(n_x^S + n_\varepsilon)} \begin{pmatrix} \mathcal{X}_{t|t-1}^{n,k,S^{(i)}} \\ \mathcal{X}_{t|t-1}^{n,k,C^{(i)}} \end{pmatrix}, \\ P_{t|t-1}^{*,n,k} &= \frac{1}{2(n_x^S + n_\varepsilon)} \sum_{i=1}^{2(n_x^S + n_\varepsilon)} \left\{ \left[\begin{pmatrix} \mathcal{X}_{t|t-1}^{n,k,S^{(i)}} \\ \mathcal{X}_{t|t-1}^{n,k,C^{(i)}} \end{pmatrix} - \begin{pmatrix} m_{t|t-1}^{n,k,S} \\ m_{t|t-1}^{n,k,C} \end{pmatrix} \right] \left[\begin{pmatrix} \mathcal{X}_{t|t-1}^{n,k,S^{(i)}} \\ \mathcal{X}_{t|t-1}^{n,k,C^{(i)}} \end{pmatrix} - \begin{pmatrix} m_{t|t-1}^{n,k,S} \\ m_{t|t-1}^{n,k,C} \end{pmatrix} \right]' \right\}. \end{aligned}$$

2) Updating

(a) For each component $\{n, k\}$ form the predicted states and controls cubature points:

$$\mathcal{X}_{t|t-1}^{*,n,k,(i)} = \mu_{t|t-1}^{*,n,k} + \sqrt{P_{t|t-1}^{*,n,k}} \zeta^{(i)}, \quad i = 1, \dots, 2(n_x^S + n_x^C).$$

(b) Obtain predicted observables cubature points through the measurement equation (55):

$$\mathcal{Y}_{t|t-1}^{n,k,(i)} = A + B \mathcal{X}_{t|t-1}^{*,n,k,(i)}, \quad i = 1, \dots, 2(n_x^S + n_x^C).$$

(c) Compute predicted observables mean, covariance and cross-covariance between states and observables:

$$\begin{aligned} \bar{\mathcal{Y}}_{t|t-1}^{n,k} &= \frac{1}{2(n_x^S + n_x^C)} \sum_{i=1}^{2(n_x^S + n_x^C)} \mathcal{Y}_{t|t-1}^{n,k,(i)}, \\ \mathcal{F}_{t|t-1}^{n,k} &= \frac{1}{2(n_x^S + n_x^C)} \sum_{i=1}^{2(n_x^S + n_x^C)} \left(\mathcal{Y}_{t|t-1}^{n,k,(i)} - \bar{\mathcal{Y}}_{t|t-1}^{n,k} \right) \left(\mathcal{Y}_{t|t-1}^{n,k,(i)} - \bar{\mathcal{Y}}_{t|t-1}^{n,k} \right)' + \mathbb{V}(u_t), \\ \mathcal{P}_{t|t-1}^{n,k,xy} &= \frac{1}{2(n_x^S + n_x^C)} \sum_{i=1}^{2(n_x^S + n_x^C)} \left(\mathcal{X}_{t|t-1}^{*,n,k,(i)} - \mu_{t|t-1}^{*,n,k} \right) \left(\mathcal{Y}_{t|t-1}^{(i)} - \bar{\mathcal{Y}}_{t|t-1}^{n,k} \right)'. \end{aligned}$$

- (d) Compute Kalman gain to obtain new filtered mean and covariance for states and controls:

$$\begin{aligned}\mathcal{K}_t^{n,k} &= \mathcal{P}_{t|t-1}^{n,k,xy} \left(\mathcal{F}_{t|t-1}^{n,k} \right)^{-1}, \\ \mu_{t|t}^{*,n,k} &= \mu_{t|t-1}^{*,n,k} + \mathcal{K}_t^{n,k} \left(y_t - \bar{\mathcal{Y}}_{t|t-1}^{n,k} \right), \\ P_{t|t}^{*,n,k} &= P_{t|t-1}^{*,n,k} - \mathcal{P}_{t|t-1}^{n,k,xy} \left(\mathcal{F}_{t|t-1}^{n,k} \right)^{-1} \left(\mathcal{P}_{t|t-1}^{n,k,xy} \right)'.\end{aligned}$$

From $\mu_{t|t}^{*,n,k}$ and $P_{t|t}^{n,k,*}$ the n_x^S states entries are retained to have $m_{t|t}^{n,k}$ and $P_{t|t}^{n,k}$.

3) Weights updating

- (a) Weights are updated using Bayes' rule:

$$\tilde{w}_{t|t}^{n,k} = \frac{\tilde{w}_{t|t-1}^{n,k} \mathcal{N} \left(\mathbf{y}_t; \bar{\mathcal{Y}}_{t|t-1}^{n,k}, \mathcal{F}_{t|t-1}^{n,k} \right)}{\sum_{n=1}^{G_{t-1}} \sum_{k=1}^K \tilde{w}_{t|t-1}^{n,k} \mathcal{N} \left(\mathbf{y}_t; \bar{\mathcal{Y}}_{t|t-1}^{n,k}, \mathcal{F}_{t|t-1}^{n,k} \right)}.$$

4) Collapsing (only if $G_{t-1}K > G$)

- (a) Components weights $\tilde{w}_{t|t}^{n,k}$ are sorted in descending order.
- (b) The first G components and their respective means and covariances $m_{t|t}^{n,k}$ and $P_{t|t}^{n,k}$ are retained and their indices $\{n, k\}$ are relabeled with $1, \dots, G$.
- (c) If the smallest retained weight $\tilde{w}_{t|t}^G < \tilde{w}_{threshold}$ resampling is conducted from the G retained mixands using probabilities proportional to $\tilde{w}_{t|t}^n$, $n = 1, \dots, G$. Weights are then set to $\frac{1}{G}$.
- (d) Next period filtering weights are finally obtained by normalization:

$$w_{t|t}^n = \frac{\tilde{w}_{t|t}^n}{\sum_{n=1}^G \tilde{w}_{t|t}^n}.$$

The likelihood function is then approximated by:

$$p(\mathbf{y}_{1:T}|\theta) = \prod_{t=1}^T p(\mathbf{y}_t|\mathbf{y}_{1:t-1}; \theta) \approx \prod_{t=1}^T \mathcal{N}(\mathbf{y}_t; \bar{\mathcal{Y}}_{t|t-1}, \mathcal{F}_{t|t-1}), \quad (62)$$

where $\bar{\mathbf{y}}_{t|t-1} = \sum_{k=1}^K \sum_{n=1}^{G_{t-1}} \tilde{w}_{t|t-1}^{n,k} \bar{\mathbf{y}}_{t|t-1}^{n,k}$ and:

$$\mathcal{F}_{t|t-1} = \sum_{k=1}^K \sum_{n=1}^{G_{t-1}} \tilde{w}_{t|t-1}^{n,k} \left[\mathcal{F}_{t|t-1}^{n,k} + \left(\bar{\mathbf{y}}_{t|t-1}^{n,k} - \bar{\mathbf{y}}_{t|t-1} \right) \left(\bar{\mathbf{y}}_{t|t-1}^{n,k} - \bar{\mathbf{y}}_{t|t-1} \right)' \right].$$

Appendix D: The Approximate Conditional Optimal Particle Filter

The Conditionally Optimal Particle Filter (COPF), see [Herbst and Schorfheide \(2015\)](#) and [Aruoba et al. \(2021\)](#), requires an exact expression for conditionally-optimal proposal density. This can be easily derived just in few special cases including: linear state transitions and piecewise-linear state transitions. Specifically, [Aruoba et al. \(2021\)](#) show that when the DSGE solution produces piecewise-linear state transition equations, the conditionally optimal density takes the form of truncated normal mixtures.

In our model solution, the state transition is a second order polynomial in the states and, unfortunately, an exact expression for the conditionally optimal density is not available and the COPF cannot be applied. As an approximation, we propose the Approximate Conditionally Optimal Particle Filter (ACOPF) which the conditionally-approximate density is derived with a CKF step. More specifically:

$$p(\mathbf{x}_t | \mathbf{x}_{t-1}^j, \mathbf{y}_t) \approx \tilde{p}(\mathbf{x}_t | \mathbf{x}_{t-1}^j, \mathbf{y}_t) = \mathcal{N} \left(\mathbf{x}_{t|t}^{j,CKF}, P_{t|t}^{j,CKF} \right),$$

where $\mathbf{x}_{t|t}^{j,CKF}$ and $P_{t|t}^{j,CKF}$ represent respectively the filtered means and covariances, of the unobserved states, obtained from a run of the CKF on the latest observation \mathbf{y}_t , this filter is also known as Cubature Particle Filter (CPF).

In the context of DSGE models, the optimal importance density approximation using Gaussian filters have been proposed, among others, by [Amisano and Tristani \(2010\)](#) (Extended Kalman Filter) and by [Andreasen \(2011\)](#) (Central Difference Kalman filter). By using an importance density proposal $g_t(\mathbf{x}_t | \mathbf{x}_{t-1}^j, \mathbf{y}_t) \neq p(\mathbf{x}_t | \mathbf{x}_{t-1}^j)$, the importance weight

$$w_t^j = \frac{p(\mathbf{y}_t | \mathbf{x}_t^j) p(\mathbf{x}_t^j | \mathbf{x}_{t-1}^j)}{g_t(\mathbf{x}_t^j | \mathbf{x}_{t-1}^j, \mathbf{y}_t)},$$

must be evaluated. In our case, as in [Andreasen \(2011\)](#), the density $p(\mathbf{x}_t^j | \mathbf{x}_{t-1}^j)$ is degenerate, given that the shocks enter contemporaneously for just some state variables, i.e. the loading matrix R displays null lines and $R\mathbb{V}(\varepsilon_t)R'$ is singular. To circumvent this problem, exactly as in [Andreasen \(2011\)](#), the proposal is split in two parts. The first one propagates the states corresponding to the singular lines deterministically through the transition functions. The second part updates the states corresponding to the non-singular lines by a run of the CKF. The importance weight for each particle is then calculated only evaluating the non-degenerate part of the density corresponding to the non-degenerate states.

Appendix E: Further results

Table 4: Full table. RMSE of the Monte Carlo experiment for $N = 100$ replications of the Two-Sector model with large shocks. The Table reports the full name (Full Name) with the associated symbol (Symbol). The filters are: Kalman filter (KF); Bootstrap Particle Filter with 40000 particles (BPF); Auxiliary Particle Filter with 40000 particles (APF); the Approximate Optimal Particle Filter with 400 and 4000 particles (ACOPF(400), ACOPF(4000)); and the Mixture of Mixture of Cubature Kalman Filter (MM-CKF) with four components ($G_t = 4$).

Full Name	Symbol	KF	BPF	APF	ACOPF(400)	ACOPF(4000)	MM-CKF
Wage \mathcal{S}_1	w_1	0.31	0.69	0.49	0.36	0.28	0.28
Int. rate	r_{not}	0.03	0.16	0.05	0.04	0.01	0.01
Lab. Supply \mathcal{S}_1	a_{t_1}	0.54	1.30	0.64	0.52	0.37	0.37
Wage \mathcal{S}_2	w_2	1.10	2.50	1.80	1.20	1.10	1.10
Lab. supply \mathcal{S}_2	a_{t_2}	1.80	2.60	2.40	1.80	0.99	0.95
Prod. \mathcal{S}_1	a_{z_1}	0.19	0.52	0.32	0.22	0.17	0.17
Prod. \mathcal{S}_2	a_{z_2}	0.60	1.40	1.00	0.64	0.59	0.59
Intertemp. shock	a_ζ	0.26	0.89	0.40	0.24	0.23	0.23
Intratemp. shock	a_j	0.46	0.94	0.75	0.49	0.38	0.38
MP shock	ϵ_e	0.02	0.03	0.03	0.03	0.01	0.01
Investment	$invest$	0.20	0.72	0.33	0.21	0.16	0.16
Total output	GDP	0.77	2.10	1.30	0.81	0.64	0.64
Hours \mathcal{S}_1	n_1	0.18	0.54	0.25	0.20	0.16	0.16
Markup \mathcal{S}_1	X_1	0.04	0.20	0.06	0.05	0.03	0.03
Hours \mathcal{S}_2	n_2	0.03	0.07	0.04	0.03	0.02	0.02
Marg. ut. \mathcal{S}_2	uc_2	0.20	0.44	0.30	0.22	0.19	0.19
Markup \mathcal{S}_2	X_2	0.04	0.20	0.05	0.04	0.02	0.02
Inflation	π	0.01	0.07	0.01	0.01	0.00	0.00
Profits retailers	Π_r	0.21	0.83	0.35	0.25	0.15	0.15
Cap. adj. Cost	Ψ_k	0.01	0.05	0.01	0.01	0.00	0.00
Wage markup \mathcal{S}_1	X_{w_1}	0.18	0.48	0.26	0.22	0.15	0.15
Wage markup \mathcal{S}_2	X_{w_2}	1.60	2.20	1.90	1.70	0.94	0.93
Profits unions	Π_u	0.64	1.80	0.73	0.67	0.25	0.25
Int. rate	R	0.02	0.06	0.02	0.02	0.00	0.00
Notional int. rate	R_{not}	0.03	0.16	0.05	0.05	0.01	0.01
Production \mathcal{S}_1	Y_1	0.71	2.00	1.30	0.77	0.59	0.59
Production \mathcal{S}_2	Y_2	0.15	0.33	0.23	0.15	0.14	0.14
Marg. ut. \mathcal{S}_1	uc_1	0.06	0.24	0.06	0.04	0.04	0.04
Rental rate \mathcal{S}_1	rk_1	0.00	0.01	0.00	0.00	0.00	0.00
Utilization \mathcal{S}_1	uk_1	0.11	0.35	0.14	0.11	0.09	0.09
Rental rate \mathcal{S}_2	rk_2	0.01	0.02	0.01	0.01	0.01	0.01
Utilization \mathcal{S}_2	uk_2	0.25	0.64	0.40	0.29	0.23	0.23
Wage infl. \mathcal{S}_1	ω_1	0.01	0.08	0.02	0.02	0.01	0.01
Wage infl. \mathcal{S}_2	ω_2	0.01	0.05	0.01	0.01	0.00	0.00
Utiliz. adj.cost \mathcal{S}_1	Ψ_{u_1}	0.00	0.01	0.00	0.00	0.00	0.00
Utiliz. adj.cost \mathcal{S}_2	Ψ_{u_2}	0.01	0.02	0.01	0.01	0.01	0.01
Consumption \mathcal{S}_1	c_1	0.52	1.60	0.95	0.56	0.47	0.47
Inflation \mathcal{S}_1	π_1	0.01	0.07	0.02	0.01	0.00	0.00
Consumption \mathcal{S}_2	c_2	0.15	0.33	0.23	0.15	0.14	0.14
Inflation \mathcal{S}_2	π_2	0.01	0.06	0.01	0.01	0.00	0.00
Capital \mathcal{S}_1	k_1	6.70	14.00	10.00	6.90	6.00	6.00
Capital \mathcal{S}_2	k_2	1.30	2.90	2.10	1.60	1.30	1.30
Relative price	p_2	0.48	1.00	0.74	0.55	0.47	0.47

Research Papers 2021



- 2020-12: Anine E. Bolko, Kim Christensen, Mikko S. Pakkanen and Bezirgen Veliyev: Roughness in spot variance? A GMM approach for estimation of fractional log-normal stochastic volatility models using realized measures
- 2020-13: Morten Ørregaard Nielsen and Antoine L. Noël: To infinity and beyond: Efficient computation of ARCH(∞) models
- 2020-14: Charlotte Christiansen, Ran Xing and Yue Xu: Origins of Mutual Fund Skill: Market versus Accounting Based Asset Pricing Anomalies
- 2020-15: Carlos Vladimir Rodríguez-Caballero and J. Eduardo Vera-Valdés: Air pollution and mobility in the Mexico City Metropolitan Area, what drives the COVID-19 death toll?
- 2020-16: J. Eduardo Vera-Valdés: Temperature Anomalies, Long Memory, and Aggregation
- 2020-17: Jesús-Adrián Álvarez, Malene Kallestrup-Lamb and Søren Kjærsgaard: Linking retirement age to life expectancy does not lessen the demographic implications of unequal lifespans
- 2020-18: Mikkel Bennedsen, Eric Hillebrand and Siem Jan Koopman: A statistical model of the global carbon budget
- 2020-19: Eric Hillebrand, Jakob Mikkelsen, Lars Spreng and Giovanni Urga: Exchange Rates and Macroeconomic Fundamentals: Evidence of Instabilities from Time-Varying Factor Loadings
- 2021-01: Martin M. Andreasen: The New Keynesian Model and Bond Yields
- 2021-02: Daniel Borup, David E. Rapach and Erik Christian Montes Schütte: Now- and Backcasting Initial Claims with High-Dimensional Daily Internet Search-Volume Data
- 2021-03: Kim Christensen, Mathias Siggaard and Bezirgen Veliyev: A machine learning approach to volatility forecasting
- 2021-04: Fabrizio Iacone, Morten Ørregaard Nielsen and Robert Taylor: Semiparametric Tests for the Order of Integration in the Possible Presence of Level Breaks
- 2021-05: Stefano Grassi and Francesco Violante: Asset Pricing Using Block-Cholesky GARCH and Time-Varying Betas
- 2021-06: Gloria González-Rivera, Carlos Vladimir Rodríguez-Caballero and Esther Ruiz Ortega: Expecting the unexpected: economic growth under stress
- 2021-07: Matei Demetrescu and Robinson Kruse-Becher: Is U.S. real output growth really non-normal? Testing distributional assumptions in time-varying location-scale models
- 2021-08: Luisa Corrado, Stefano Grassi and Aldo Paolillo: Modelling and Estimating Large Macroeconomic Shocks During the Pandemic